BRNO UNIVERSITY OF TECHNOLOGY
VYSOKÉ UČENÍ TECHNICKÉ V BRNĚ

FACULTY OF MECHANICAL ENGINEERING
FAKULTA STROJNÍHO INŽENÝRSTVÍ

INSTITUTE OF SOLID MECHANICS, MECHATRONICS AND BIOMECHANICS
ÚSTAV MECHANIKY TĚLES, MECHATRONIKY A BIOMECHANIKY

CONSTRAINED MODELING OF INDUCTION MOTOR USING PHYSICAL MODELING AND FEM
VÁZANÉ MODELOVÁNÍ ASYNCHRONNÍHO MOTORU METODOU FYZIKÁLNÍHO MODELOVÁNÍ A METODY KONEČNÝCH PRVKŮ

MASTER'S THESIS
DIPLOMOVÁ PRÁCE

AUTHOR   Bc. Tomáš Trávníček
AUTOR PRÁCE

SUPERVISOR   doc. Ing. Radek Vlach, Ph.D.
VEDOUCÍ PRÁCE

BRNO 2017

Master's Thesis Assignment

Institut:	Institute of Solid Mechanics, Mechatronics and Biomechanics
Student:	**Bc. Tomáš Trávníček**
Degree programm:	Applied Sciences in Engineering
Branch:	Mechatronics
Supervisor:	**doc. Ing. Radek Vlach, Ph.D.**
Academic year:	2016/17

As provided for by the Act No. 111/98 Coll. on higher education institutions and the BUT Study and Examination Regulations, the director of the Institute hereby assigns the following topic of Master's Thesis:

Constrained Modeling of Induction Motor Using Physical Modeling and FEM

Brief description:

The design of induction machine consists of several partial models as electromagnetic, thermal, mechanic and possibly others that are solved separately. Models influence each other; therefore, the whole design needs to be revised.

The goal is to create a lumped-parameter model of induction machine that includes electromagnetic and thermal models. These models are mutually interacted by themselves depending on a variation of machine parameters. Both — a method of physical modelling based on a circuit modelling of physical principles in the induction machine and the FEM method for calculating electromagnetics — should be used to achieve the goal.

Master's Thesis goals:

1. Literature research
2. Design of electromagnetic model of induction machine
3. Design of thermal model of induction machine
4. Design of lumped-parameter model of induction machine
5. Evaluation of simulation results

Recommended bibliography:

Yunus, A., Turner, H., Cimbala, J.M.: Fundamental of Thermal-fluid Sciences. 3rd edition. McGraff Fill: Anstralia & New Zeland, 2008.

Hak, J., Ošlejšek, O.: Výpočet chlazení elektrických strojů. 1.díl. VUES Brno, 1973.
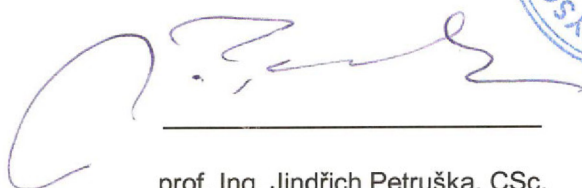
Ondruška, E., Maloušek, A.: Ventilace a chlazení elektrických strojů točivých. SNTL Praha, 1985.

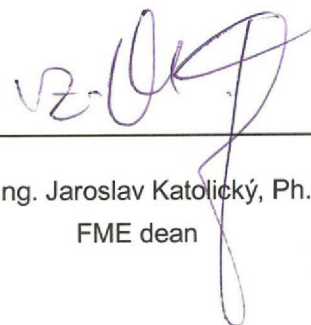Pavelka, J., Čerovský, Z., Javůrek, J.: Elektrické pohony, skriptum ČVUT.

Pešek, M.: Program FEMM – podklady pro výuku v elektronické formě, Brno: FEKT VUT v Brně, 2009, 54s, bakalářská práce.

Students are required to submit the thesis within the deadlines stated in the schedule of the academic year 2016/17.

In Brno, 4. 11. 2016

L. S.

_____
prof. Ing. Jindřich Petruška, CSc.
Director of the Institute

_____
doc. Ing. Jaroslav Katolický, Ph.D.
FME dean

Abstract

This thesis deals with the design of a complex model of induction machine whereby an analysis of such machine can be performed. The whole model consists of several sub-models such as electromagnetic, electric and thermal. The electromagnetic sub-model is solved via finite element analysis provided by a program called *FEMM*. Further computations have been executed via *Matlab*. The thermal sub-model is designed for a steady-state of the machine at the desired operating point. The electric model represents an electric circuit which models the relations of electric quantities. The final combined model has been programmed in *Matlab* as a tool for analyzing the induction machine.

Keywords

Induction machine, FEA, FEMM, heat transfer, lumped-parameter system

Abstrakt

Tato práce řeší návrh komplexního modelu asynchronního stroje, pomocí něhož se dá stroj analyzovat. Model se skládá z dílčích modelů, které popisují asynchronní stroj z hlediska elektromagnetického, elektrického a tepelného. Elektromagnetický model je řešen pomocí metody konečných prvků v programu zvaném *FEMM*. Další výpočty jsou provedeny pomocí *Matlabu*. Tepelný model počítá s ustáleným stavem stroje v požadovaném pracovním bodě. Elektrický model je řešen pomocí náhradního schématu, ze kterého jsou odvozeny vztahy pro elektrické veličiny. Výsledný propojený model je naprogramován v *Matlabu* a slouží jako nástroj pro analyzování asynchronního stroje.

Klíčová slova

Asynchronní stroj, FEA, FEMM, přenos tepla, systém s vázanými parametry

Bibliographic citation

TRÁVNÍČEK, T. *Constrained Modeling of Induction Motor Using Physical Modeling and FEM.* Brno: Brno University of Technology, Faculty of Mechanical Engineering, 2017. 64 pages. Leader of Master thesis doc. Ing. Radek Vlach, Ph.D.

Statement

I affirm that the presented master's thesis is my original work and that it was created with the support of the stated literature, under the supervision of my tutor.

Trávníček Tomáš, Brno, 2017

....

Acknowledgements

Contents

1 Introduction

Recently, there is a modern trend that puts more emphasis on saving energy and safety. This work deals with the analysis of an induction machine. The aim is to get maximum performance of the electrical machine nearly to its limits. It is essential to know where these limits are. However, it is even possible to exceed these limits but only for a short time. When the machine is overloaded, the temperature becomes high, and therefore it can burn. This work was targeted on creating a model of such an engine.

The solution of the model deals with magnetism, heat transfer and the electric circuit. It combines several software tools and it is suitable for variable types of engines. It has a user interface which is easily used. The model is actually a program that communicates with the software named *FEMM* several times over. *FEMM* uses the finite element method to solve complicated physical equations in order to get specific quantities of the engine. It is necessary to perform computations in *FEMM* for various situations; therefore, the program in *Matlab* was meant to take care of the communication with *FEMM*.

A work that encounters modeling an induction machine in *FEMM* was written by David Meeker [4]. Since *FEMM* can be used for computation of *2D* problems only, the machine must be simplified and transferred from *3D* into *2D* configuration. Also, it is not (yet) possible to do simulation of an induction machine while running. Hence, the analysis must be done under specific conditions at zero speed. Although there is a lot to be attained to in the future, one can still obtain relatively realistic results.

2 Theoretical survey

In order to model the machine, a literature research of the important aspects has been carried out. General research about the induction machine is in section 2.1. The section deals with the construction, functionality, controlling and expressing its mechanical quantities in terms of an electric power supply. Next, section 2.2 deals with magnetism of linear and nonlinear materials. Section 2.3 then continues from the previous sections and deals with modeling induction machine using *FEMM*. The last section, 2.4, is addressed to heat transfer and a method of modeling a thermal system.

2.1 Induction machine

This section deals with the basic constitution of an ordinary induction machine. The machine is described from different points of view in order to define basic relations between the machine properties and physical quantities that occur inside.

2.1.1 Basics of an induction machine

Typical induction machines generally consist of a stator, rotor, casing and cooling device. An example of such a machine is shown in figure 2.1. The rotor has two different parts. The first of them is the core which is usually made from a ferromagnetic metal. The second is the rotor cage which is made from a conductive metal. The cage (also known as a *squirrel cage*) consists of many rotor bars which lead through the rotor core as well as of rotor end-rings which are outside the core. Also, the rotor is joined to a shaft which is the output of the entire machine and which is joined using some bearings to the casing. The stator surrounds the rotor and is fixed to the casing. It also consists of a ferromagnetic core and conductors that lead through the core in slots. These conductors form coils with a lot of turns that need to be connected to one another and thus there is significant stator end-wiring. Additionally, the machine is usually cooled with a fan joined to the shaft or with another cooling device possibly including various coolants. The rotor can be potentially more complicated. For example it can include coils instead of bars or the bars can be found within more layers or skewed etc. The whole concept can involve some additional devices such as sensors and others; however, this is only a brief description of such a machine.
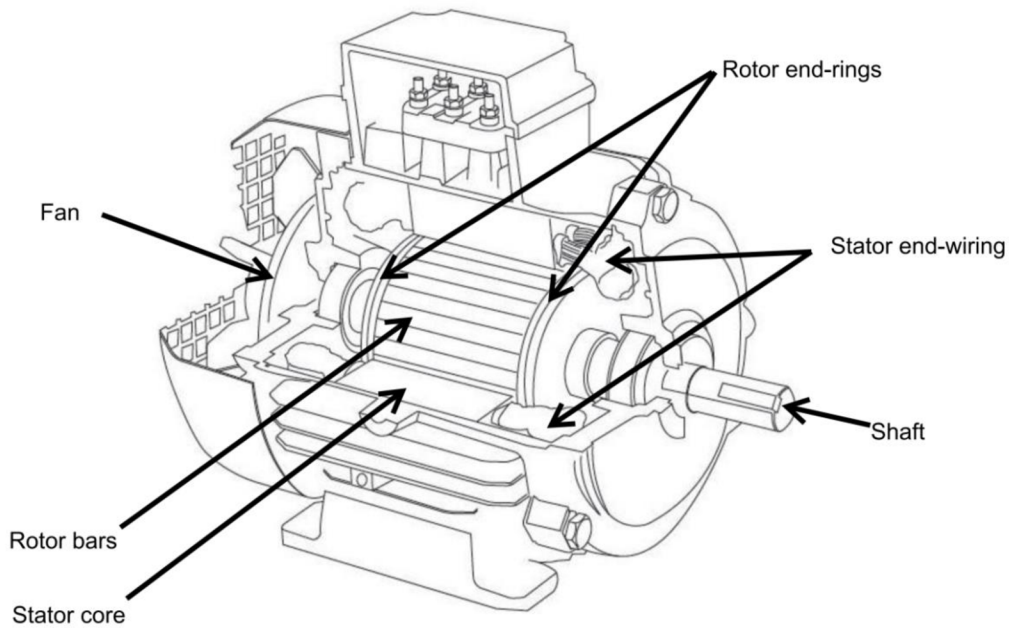
Figure 2.1: Composition of an induction machine [1]

The stator is meant to create a rotating magnetic field. For that reason, most common machines are constructed with a three-phase *AC* power supply which can create it easily and effectively. While measuring the voltage, each phase has *120°* angle between the two others. Each phase is wired into coils that create magnetic induction. The situation is visualized in figure 2.2. The figure shows three axis in one moment, representing the three phases. On the right side of the picture we can see three *phase-inductions*: B_x, B_y and B_z. The total *induction B* (dashed) is the sum of all inductions created by all phases. On the left side of the picture we can see the stator with slots for the winding. There are also the inductions with the *120°* angle between them. One can see the field in this figure creates exactly two poles. Nevertheless, the stator can be constructed with any even number of poles. In that case, the rotation speed of the rotor differs depending on the frequency of power supply voltage and on the number of poles. Defining p as the number of pole pairs and f as a frequency of power supply we can express some speed quantities. The *electrical angular velocity* can be expressed as

$$\omega = 2\pi f \tag{2.1}$$

Including the number of poles, the maximal rotor speed can be expressed as

$$\omega_{r,max} = \frac{\omega}{p} \tag{2.2}$$

The rotating magnetic field induces currents in the rotor cage. This fact leads to inducing a second rotating magnetic field due to the currents in rotor bars. At on-load steady state, the velocity difference between these two rotating fields can be expressed as

$$\omega_s = \omega - p \cdot \omega_r \tag{2.3}$$

The final rotating magnetic field generates torque and thus it transfers electric energy from the stator into mechanical energy in the rotor.
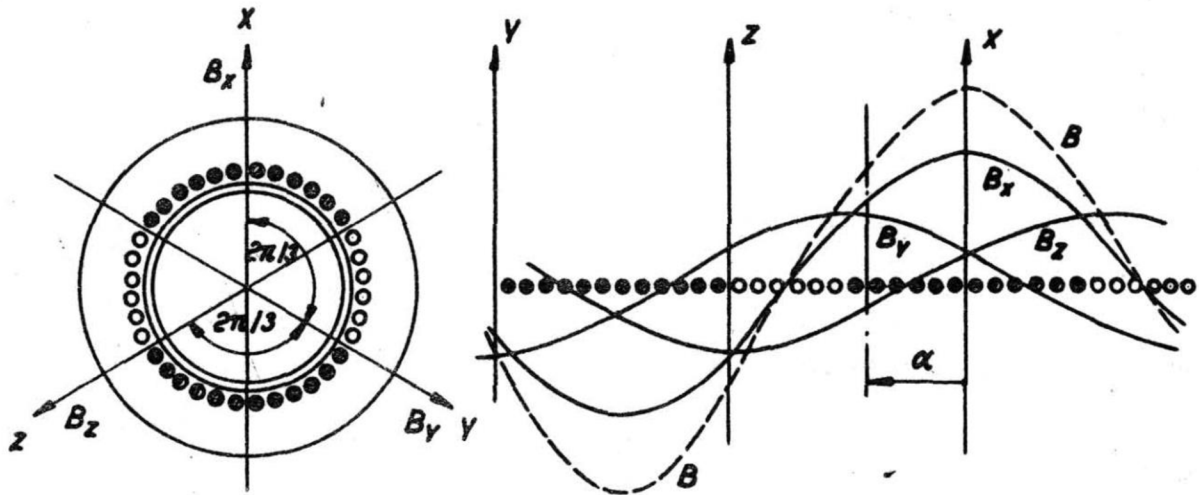
Figure 2.2: Rotating magnetic field [2]

2.1.2 Electrical schema

According to [3], the electrical part can be modeled using an electrical schema. Using the schema we can express impedances and currents flowing through each electrical branch in terms of a power supply. A general schema related to one phase is shown in figure 2.3. The electrical circuit in the schema can be divided into a left, right and middle branch. The left represents a stator winding and the right represents a rotor winding. The middle one represents the reaction between the stator and the rotor including losses in cores. The boxes represent the *impedances*. The R_s represents re*sistance* of the stator and the L_l represents *leakage inductance* of stator winding. L_{l2} is *leakage inductance* of the rotor and R_r represents the *resistance* of the rotor as well as the power consumption of the shaft which is related to the rate between the power supply frequency and the slip frequency. R_{Fe} is like a power consumer which stands for iron core losses caused by eddy currents, magnetization losses and possibly more. The *M* is a *mutual inductance* between stator and rotor.
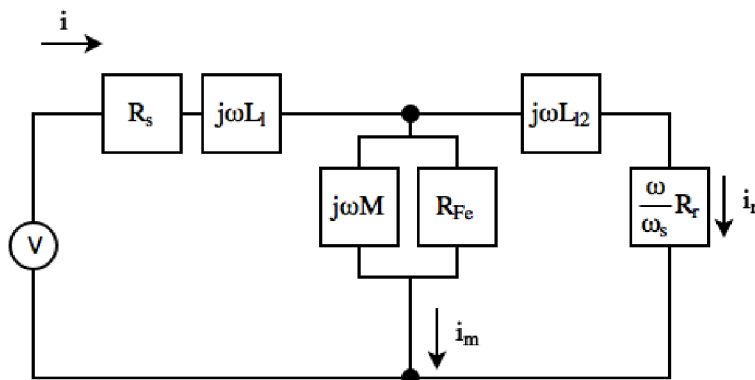

Figure 2.3: General electrical schema

Considering the rotor cage as a simple cage with bars, we can claim that the *leakage inductance L_{l2}* of the cage is negligible. As we neglect also the iron losses, we can simplify the model into that in figure 2.4 as proposed in [4].
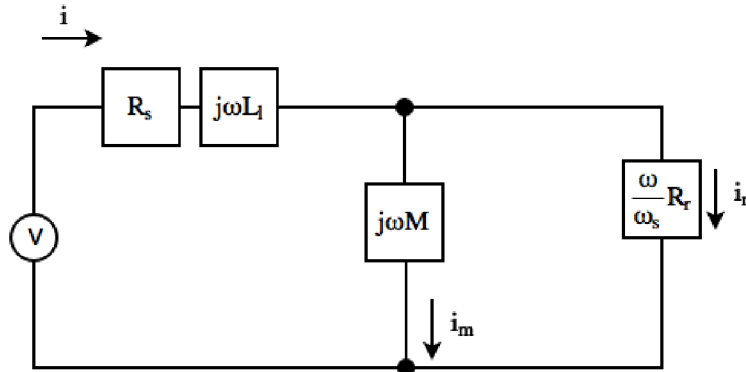

Figure 2.4: Simplified electrical schema

We can express the current i using the *overall impedance Z*.

$$i = \frac{v}{Z} \tag{2.4}$$

where v is *phase voltage*. Following the approach in [4], the *impedance* can be further expressed as

$$Z = R_s + j\omega \left(L_l + M \cdot \frac{1}{1 + j\tau\omega_s} \right) \tag{2.5}$$

where τ is a rate between M and R_r.

2.1.3 Behavior and control

According to equation 2.2, the maximal speed is dependent on the frequency of the power supply. The real steady-state speed is a little bit lower than the maximal, usually 95% or more. Considering this fact, it is difficult to control the speed. Thus, these machines are broadly used for applications with more or less constant speed. Despite this restriction, the speed can be smoothly controlled using an additional device called a variable-frequency drive or can be controlled within certain speeds using other methods. However, this work deals with widely used constant frequency. The advantages of this machine are above all its efficiency and lifespan. The efficiency is related to the *output power* and according to [4] it can be expressed as

$$P_{mech} = 3 \left(\frac{p\omega_r}{\omega_s} \right) R_r |i_r|^2 \tag{2.6}$$

where i_r is the *current* flowing through the rotor cage related to one stator phase. Dividing by the *rotor angular velocity* we can get an expression of *torque*

$$T = \frac{3pR_r}{\omega_s} |i_r|^2 \tag{2.7}$$

A sample of the relation between torque and a rotor current over slip frequency is shown in figure 2.5.
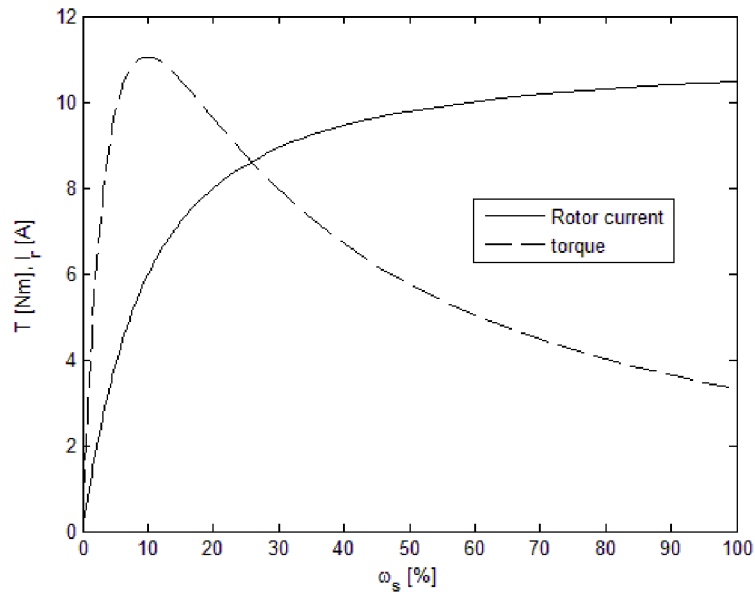
Figure 2.5: Torque and rotor current over slip frequency

On the left side of the graph, when the slip frequency is zero, the machine is at its maximum speed. On the other side of the graph, when the slip frequency is at its maximum, the machine is totally stopped. As stated above, the machine usually works within a range from 95% to nearly 100% speed and that corresponds to 0 to 5% of slip frequency as shown in the graph. One can judge that having the machine stopped leads to enormous current. Nevertheless, the machine needs to be started anyway and according to the fact the current is very high the starting must be quick because the heat, dissipated by the resistance, is proportional to the square of the current. Taking these facts into account, we can see why it is so difficult to control the velocity.

As the rotor temperature rises, the resistance increases as well in the case of the stator. This rise can strongly change machine behavior as can be seen in figure 2.6.

Figure 2.6: Different rotor resistances

When the rotor resistance gets higher, the same value of torque is reached at a higher slip frequency, i.e. lower speed. Considering that the output power is a multiplication of both torque and speed, the output power gets even lower. Another special thing about increased rotor resistance is that the torque at zero sp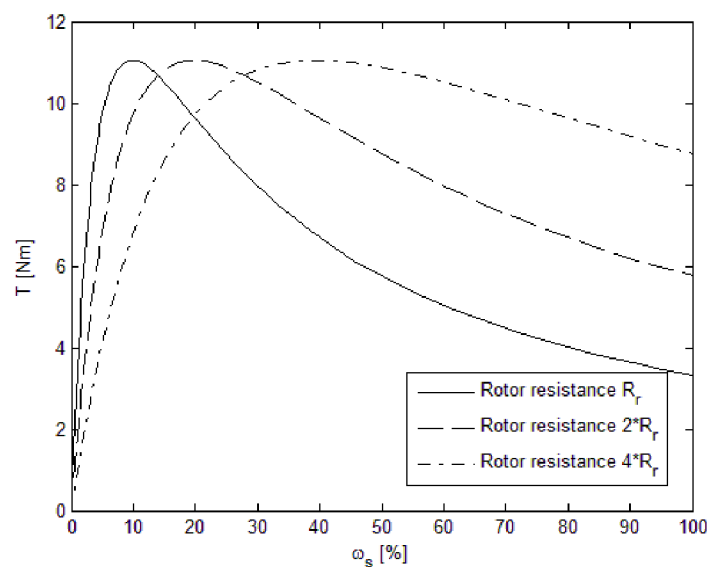eed (max. slip frequency) is also increased. This fact is used when the machine is about to be started when being on-load.

2.1.4 Energy balance and losses

Following the law of conservation of energy, we can define the energy flow. The output power together with the losses equals the input power. This relation is valid only when the machine is at steady-state and no energy accumulates in the machine. The input power is a real part of the electric power given from the power supply. Losses are related to the stator and rotor as in figure 2.7. In the figure, the stator and rotor are separated with a double-line which stands for an air gap between them.
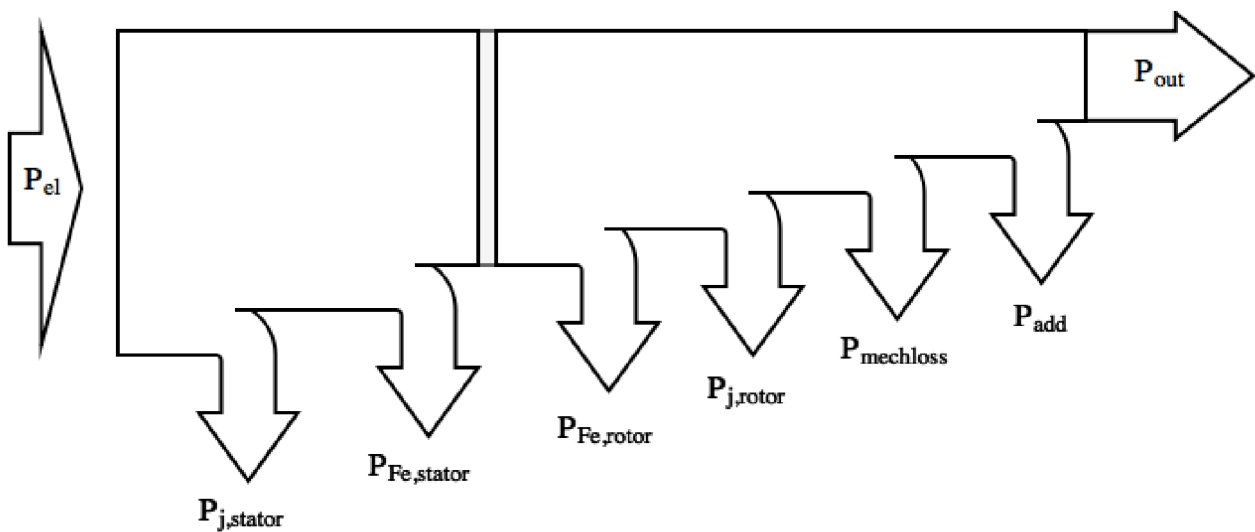

Figure 2.7: Schema of energy flow

The $P_{j,stator}$ and $P_{j,rotor}$ are produced due to joule losses in stator winding and rotor cage and they represent major heat losses. The $P_{Fe,stator}$ and $P_{Fe,rotor}$ are produced due to magnetization of the stator and rotor core. More about the magnetization losses is discussed in section 2.2. The $P_{mechloss}$ is produced due to mechanical friction. The P_{add} are additional losses. There are several other types of losses, e.g. surface losses, high-harmonic losses and more, which can be unified into the additional losses. Without exception, all the losses are transformed into heat. The whole balance can be expressed as

$$P_{el} = P_{j,stator} + P_{Fe,stator} + P_{Fe,rotor} + P_{j,rotor} + P_{mechloss} + P_{add} + P_{out} \qquad (2.8)$$

Rotating at nominal speed, the losses can be either significant or negligible. For example, the rotor core losses are proportional to derivative of induction inside it. As the slip frequency is low, the frequency of alternating the induction is also low and thus these losses are low at nominal speed, but on the other hand, they are maximal at zero speed. In the case of mechanical losses, a major part of friction depends on actual speed. In the case of fluid friction (usually a fan), the losses depend on a square of the actual speed. Thus they can usually be neglected at the starting of the machine. The mentioned losses (except the joule) are more or less significant and therefore it is up to the designer to take them into account.

2.1.5   Additional parameters of an induction machine

As mentioned above, the machine can be constructed to create any even number of poles. The number of pole pairs depends on the configuration of stator winding. Considering there are three phases and each needs to go back and forth through the core, the number of stator core slots must be exactly a multiple of 6. The position of the slots and their count defines the number of the pole pairs. The number of stator slots is called Q_1. The rotor sees the number of poles rather than the number of phases and thus it is usually built in a multiple count of poles. The number of rotor slots is called Q_2. The configuration of stator phases can be various. For example, when there are 6 slots with three phases and we double the number of slots to 12 we can either put each new winding beside the same slot or put the new winding in the opposite slot. In the case of the first placing, we do not increase the number of poles. For example, the stator winding in figure 2.2 has new windings side by side in a group and the stator still creates two poles. In the case of the second placing, when we double the number of slots the number of poles will be doubled as well.

Another construction parameter is the connection of the phases to the power supply. There are two types of connection – the *delta* and the *wye* configuration. The difference between them is above all in amplitude of the voltage. When wye connected, the voltage is lower and according to equation 2.4 the current is also lower. Unfortunately the torque is dependent on the current and thus it will drop. This fact is useful when the machine starts with no-load state. If the configuration is changeable and the machine has sped up to the nominal speed we can easily turn it to *delta*-wired configuration whereby the torque gets higher.

2.2 Electromagnetism

This section deals with expressing basic equations in electromagnetism and the behavior of metal materials.

2.2.1   Basic principles

Comprehensive academic materials regarding electromagnetism are presented in [5]. The cores are made of ferromagnetic materials which enable to be magnetised at the utmost. At first we recall Faraday's law. A magnet entering a coil produces a *voltage* which is proportional to a derivative of *magnetic flux* as in equation 2.9.

$$v = N \frac{d\phi}{dt} \tag{2.9}$$

where N is the number of turns in the coil. We can modify this equation into a harmonic wave form of flux as in equation 2.10.

$$v = \sqrt{2} \cdot \pi \cdot N \cdot f \cdot \phi_{max} = 4.44 \cdot N \cdot f \cdot \phi_{max} \tag{2.10}$$

The *square root of 2* is there because of the *root mean square* of the *harmonic flux* and the time period $2\pi f$. According to [2] and [3], the *induced voltage* in the stator is usually refined using a *winding fill factor* k_w as follows

$$v = 4.44 \cdot N \cdot f \cdot \phi_{max} \cdot k_w \tag{2.11}$$

The factor is calculated with respect to both the winding configuration (section 2.1.5) and other aspects of winding position and thereby it lowers the ideal flux. A detailed approach of an estimation of this factor is in [6].The flux can be further expressed in terms of *magnetic flux density B* as

$$\phi_{max} = B_{max} \cdot A_e \tag{2.12}$$

where A_e is an *effective core area*. The *magnetic flux density* is related to the *magnetic field strength* via *permeability* of the material μ.

$$B = \mu \cdot H \tag{2.13}$$

The *permeability* is usually defined as the *relative permeability* related to the *absolute permeability* of vacuum $\mu_0 = 4\pi \cdot 10^{-7} NA^{-2}$ as in equation 2.14.

$$\mu_r = \mu/\mu_0 \tag{2.14}$$

The *magnetic field strength* can be described in the case of a straight wire with a current flowing therein. The electrons moving inside the wire create a magnetic field with *magnetic field strength H* which is proportional to the current. *H* can be expressed as

$$H = \frac{I}{2\pi r} \tag{2.15}$$

The magnetic flux can also be expressed in terms of a current flowing through a coil with known *inductance L* as

$$d\phi = \frac{L \cdot di}{N} \tag{2.16}$$

When substituting equation 2.16 into equation 2.9 we can express the *voltage* of the coil as

$$v = L \cdot \frac{di}{dt} \tag{2.17}$$

2.2.2   Non-ideal materials

Usually, real materials used in the machine cores do not obey equation 2.13 because the *permeability* is not a constant value. In this particular case, the value of *permeability μ* follows the equation 2.18 as in [7]. The function $H(B)$ is specific for each material and the manufacturer usually provides it.

$$\mu = \frac{B}{H(B)} \tag{2.18}$$

The relation of *H* and *B* is shown in figure 2.8. According to [8], the curve is not straight due to the fact that there are several changes that occur inside the material. The first slow rise is due to a *reversible growth*. The steep rise is due to an *irreversible growth*. The second slow rise is a *rotation of magnetic domains* and the last very slow rise follows *paramagnetic* behavior [8]. Basically, the magnetism is explained as a lining up of the *atomic magnetic moments* in parallel with

their neighbours. Additionally, a displacement of the electrons trajectory from its original track occurs whereby the *natural moment* of molecules is changed. When the alignment is complete, and there is no longer any *magnetic moment* remaining to rotate, the material becomes saturated at the magnetic flux.
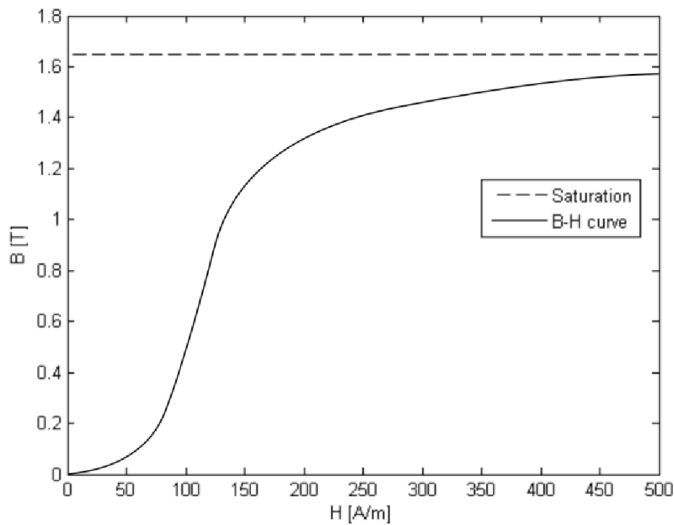

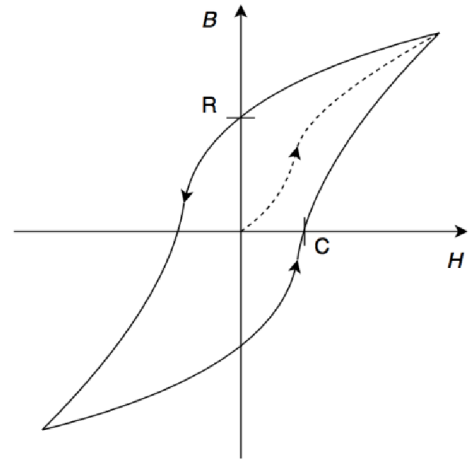Figure 2.8: Sample of non-linear material *B-H* curve   Figure 2.9: *Coercivity* and *remanence*

The ferromagnetic material has also two important abilities – *coercivity* and *remanence* – which are related to the *hysteresis effect*. *Remanence* is the ability of remaining magnetic flux after subjecting the material to a high value of magnetic field strength. *Coercivity* is the value of *magnetic field strength* that is required to reduce *remanent flux* to zero. This material behavior is parasitic when the material is used for a coil core but essential when the material is used for a magnet. Related to induction machines, there is an effort to minimize this parasitic behavior. Figure 2.8 is characterizing the property of the material itself. Figure 2.9 shows the operating state of material (unbroken line) wherein the magnetization polarity changes and the initial magnetization of the material (dashed line). The difference between figure 2.8 and 2.9 is also that the first one is an *effective B-H curve* which is just a simplification of the curve (curves) in the second figure whereby the *remanence* and *coercivity* are omitted.

The alternating magnetization and demagnetization cause a movement of intrinsic particles whereby the machine experiences it as an energy loss. Also, ferromagnetic materials are metals which are conductive in terms of electricity (good thermal conductors as well). Hence, parasitic *eddy currents* also occur when subjected to an alternating magnetic field. There are at least three methods for computing the *hysteresis loss*. One of them is in [9] where the loss depends on *frequency*, the material *hysteresis coefficient* and B^n where n is usually between 1 and 2 depending on the material. Next, the approach in [10] uses dependency on *frequency*, maximal *permeability*, the angle of the actual *B-H curve tangent* and squared *flux density* B^2. This approach is used in *FEMM* analysis. A commonly used approach rests in usage of an approximated value of losses measured while being subjected to a specific frequency and flux density, e.g. *50Hz* and *1T*. This approximated value is often provided in the material data sheet.

2.3 FEMM

According to the modern convenience of computation means, there are ways to compute the machine parameters using a finite element analysis (FEA). A component of modeling induction machines in this thesis is the program known as *Finite Element Method Magnetics* (*FEMM*).

2.3.1 Program capabilities

As described in [7], *FEMM* can solve *2D* problems including *2D* problems in radial section. Provided the problem occurs with low frequency, *FEMM* is capable of solving linear/nonlinear magnetostatic problems, linear/nonlinear time harmonic magnetic problems, linear electrostatic problems and steady-state heat flow problems. In the preprocessor editor screen one can easily draw simple geometry; however, it supports importing *dxf* files as well as the exporting of them. There is a library with a lot of various materials and we can naturally adjust its properties or even set up new ones. We can also set up electrical circuits, boundaries and groups. The model can be saved as a *fem* file.

Before the solution is done, *FEMM* divides the geometry into triangles as shown in figure 2.10. The mesh size can be either automatic or user defined.
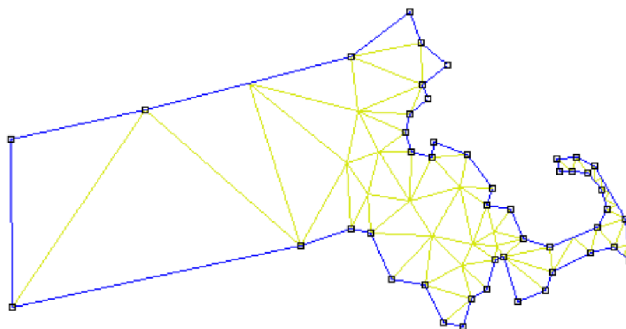

Figure 2.10: Triangulation of Massachusetts [7]

The solution consists of solving partial differential equations. The *Maxwell's equations* used for solving *2D* problems are described in [7]. The necessity of low frequency is due to neglecting the displacement currents which take place mainly at radio frequencies. The solution is designed for static problems and thus the geometry does not change during one analysis.

When the solution is done, we can scope various quantities in the model. The postprocessor editor enables one to evaluate the electric and electromagnetic quantities in the circuits as well as the electromagnetic and force quantities. These quantities can be related to geometrical entities such as points, lines, polylines, curves and areas. Density and contour of the quantities can be visualized using the density and contour plot functions in the entire area. Also, vector quantities can be visualized using the vector plot.

The program enables scripting via the *Lua* console whereby commands are instructed in sequence. This *Lua* script can be also saved in a *Lua* script file. The commands can adjust the preprocessor, solution and postprocessor properties; in addition, the editor and view commands can be changed using the *Lua* script as well.

Another way to order the commands is using the *OctaveFEMM* toolbox which uses *Active X*. This free toolbox enables putting the sequences into loops within the Matlab.

2.3.2 Analysis of induction machine using Femm

The following approach comes from an example of induction machine analysis using *FEMM* in [4], written by David Meeker. Using the postprocessor in *FEMM*, we can acquire a complex value of flux linking any phase. Considering the flux and *current* are harmonic and the flux is a *flux linkage* through all coil turns in equation 2.16, we can express their relation as

$$\Phi = L \cdot i \tag{2.19}$$

Using *FEMM* we can obtain the complex value of *flux leakage* for a given *current* and slip frequency. Thus, we can get the complex value of *inductance*. Assuming that the second term in equation 2.5 is an *inductive reactance*, we can derive its real and imaginary part as follows

$$L_r = \left(L_l + \frac{M}{1 + (\tau\omega_s)^2} \right) \tag{2.20}$$

and

$$L_i = -\left(\frac{\tau\omega_s M}{1 + (\tau\omega_s)^2} \right) \tag{2.21}$$

Rearranging equation 2.21 and substituting τ and M we get equation 2.22.

$$\omega_s \cdot c_1 + L_i \omega_s{}^2 \cdot c_2 = -L_i \tag{2.22}$$

Using the *least-square-fit* method we can solve the constants c_1 and c_2 for at least two pairs of L_i and ω_s. The *leakage inductance* L_l can be obtained using the same method. Nevertheless, the *leakage inductance* is more or less constant over the slip frequency; hence, we can use the mean of obtained values.

$$L_l = L_r - \frac{M}{1 + (\tau\omega_s)^2} \tag{2.23}$$

2.4 Designing a thermal model

Since we need to calculate the temperatures inside the working machine we must figure out the heat mechanisms that occur inside. The whole system can be substituted using a thermal net. Each node in the net represents a point in the system. The net can be viewed as a thermal circuit with heat sources and resistances.

2.4.1 Heat transfers

According to [11], there are four main ways the heat energy is transferred. Following relations are valid for a steady state of thermal quantities. Basically, the heat transfer is analogous to an electric charge transfer. The *heat flow* $\dot{Q}$ is directly proportional to the temperature difference $\Delta T = T_2 - T_1$ and inversely proportional to *thermal resistance R*. Also, heat flows from the warmer to cooler side and thus there is a *minus* representing the descending temperature along the heat flow direction.

$$\dot{Q} = -\frac{\Delta T}{R} \tag{2.24}$$

The first of heat flow mechanisms is that of **conduction in a solid material**. Having a flat wall made of a solid consistent material, we can express the *heat flow* between two different sides as

$$\dot{Q} = -kA\frac{\Delta T}{\Delta x} \tag{2.25}$$

where Δx is the thickness of the wall, A is the area of the wall and k is a *thermal conductance coefficient*. The *heat flow* can be also defined in terms of the surface wherein it flows.

$$q = \frac{\dot{Q}}{A} = -k\frac{\Delta T}{\Delta x} \tag{2.26}$$

Heat conduction through a wall is shown in figure 2.11. The temperature T_1 is higher than T_2.
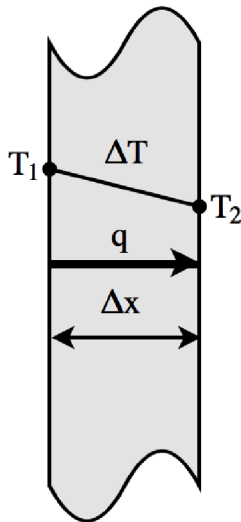

Figure 2.11: Heat conduction through a wall   Figure 2.12: Heat conduction through a cylinder
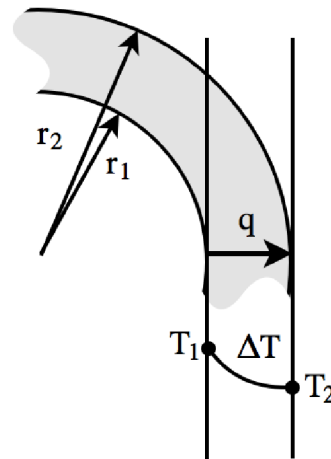
The *heat flow* through a cylinder is radius dependent, as shown in figure 2.12. Therefore, having equation 2.25 in a differential form:

$$\dot{Q} = -kA\frac{dT}{dx} \tag{2.27}$$

enables integrating it from $x = r_1$ to $x = r_2$ for distance, and from T$= T_1$ to $T = T_2$ while substituting the area A with $2\pi rL$ where L is the axial length of the subjected cylinder surface

$$\int_{r_1}^{r_2} \frac{\dot{Q}}{2\pi rL}\,dr = -\int_{T_1}^{T_2} k\,dT \tag{2.28}$$

Finally the *heat flow* yields equation 2.29.

$$\dot{Q} = -2\pi L k \frac{T_2 - T_1}{ln\left(\frac{r_2}{r_1}\right)} \tag{2.29}$$

Additionally, 2π stands for the angle of the observed *radial-cross-section area*; i.e., if we cut the cylinder imaginarily lengthwise into half we would use π instead of 2π in equation 2.29.

The next heat transfer mechanism is that of **convection**. Convection can be separated into two types – natural and forced. Both cases are possible only in a fluid medium which is in movement. The movement can be caused by either expanding the volume of a nearby fluid medium via warming or by outer force, shown in figure 2.13. *Heat flow* due to the convection is directly proportional to the area as well as to the temperature difference between the nearby surface and the cooling medium. The *convection heat flow* is expressed as

$$\dot{Q} = -hA(T_1 - T_2) \tag{2.30}$$

The h is a *convection heat transfer coefficient* which is dependent on the surface material, surface roughness, material of medium and type of medium motion and more. There is plenty of research that deals with the measurement and estimation of coefficients.

Another type of heat transfer mechanism is **radiation**. Each body which has a temperature higher than absolute zero emits thermal radiation waves. These waves can also be absorbed by other bodies. In the case of vacuum, there is no matter inside and thus there is no energy absorbed. Then, the thermal radiation can be divided in terms of direction into an absorption and emission which depends on *absorptivity* and *emissivity* respectively. Both the *absorptivity* and *emissivity* depend on the surface material and their value is in a range between 0 and 1. Heat flow out of the surface due to radiation emission yields

$$\dot{Q} = \varepsilon \sigma A T^4 \tag{2.31}$$

where ε is the *emissivity* of the surface, $\sigma = 5.67 \cdot 10^{-8} W m^{-2} K^{-4}$ is the *Stefan-Boltzmann constant* and A is the area of the surface. The *heat flow* into the surface due to radiation absorption obeys

$$\dot{Q} = \alpha \dot{Q}_{outer} \tag{2.32}$$

where α is the *absorptivity* of the surface. When the surface of a body with *temperature T_1* is surrounded by a much larger surface with *temperature T_2*, separated with air or another gas that hardly absorbs any radiation, the *heat flow* to the surrounded body follows

$$\dot{Q} = \varepsilon \sigma A \left(T_1{}^4 - T_2{}^4\right) \tag{2.33}$$

where A is the area of the surface of the surrounded body and ε is the *emissivity* of the surface. The situation is shown in figure 2.14.
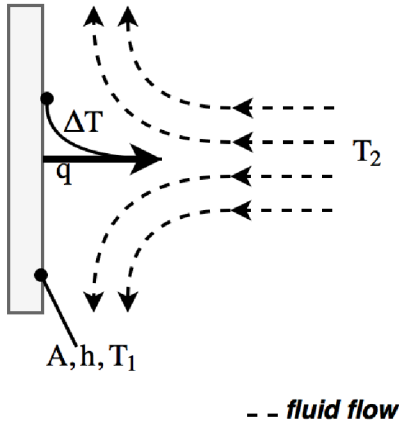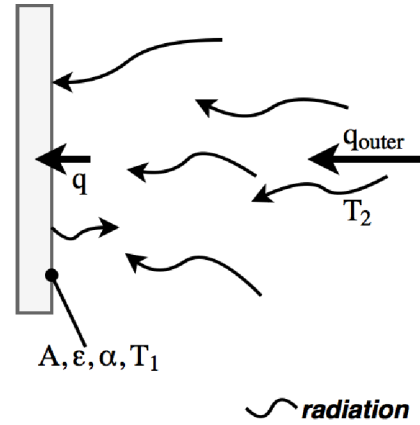
Figure 2.13: Convection

Figure 2.14: Radiation

Equation 2.33 can be also expressed in terms of temperature difference as follows

$$\dot{Q} = \varepsilon\sigma A(T_1 - T_2)(T_1 + T_2)\left(T_1^2 + T_2^2\right) \tag{2.34}$$

The fourth heat transfer mechanism is **thermal contact conduction**. The surface of two bodies being in contact is not perfectly smooth. Such an interface consists of conductive peaks and gaps filled by a medium. The *conductivity* depends on the roughness of the surfaces and the substance in the gaps. For example, a thermal conductive paste is often used between a processor and its cooler. This paste fills the gaps whereby the interface between bodies becomes even more conductive than the material of the bodies itself. *Heat flow* through the interface is expressed as

$$\dot{Q} = h_c A \cdot \Delta T \tag{2.35}$$

where A is the area of the interface, ΔT is the *edge-temperature difference* between the bodies and h_c is the *thermal contact conductance* which is experimentally determined.

2.4.2 Thermal net

The thermal system can be modeled with a thermal net representing all bodies and their connection in the system. According to equations 2.24, we can define the *resistivity* of heat flow mechanisms in equations 2.25, 2.29, 2.36 and 2.35. That means we can define the *resistance* through a body, between the body and its surrounding fluid and also between two bodies in the system. A brief example of a thermal system is shown in figure 2.15 a) which is modeled using thermal resistances in figure 2.15 b). *Overall resistance* is derived analogously as in the case of an electric circuit as follows

$$R_{combined} = \frac{R_1 \cdot R_2}{R_1 + R_2} + R_3 \tag{2.36}$$
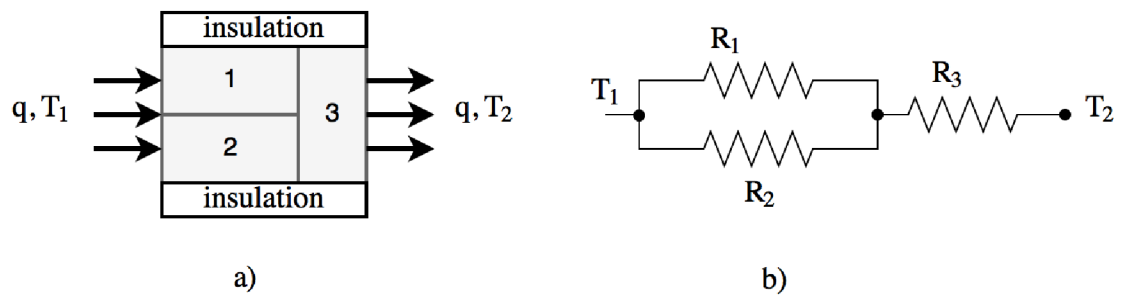
Figure 2.15: a) Modeled thermal system and b) Thermal resistances of the system

In addition, the heat flow from body 1 to 3 and from 2 to 3 could be further specified by adding some extra resistors representing the *thermal conduct conductance* between the mentioned bodies.

3 Objectives

The model of an induction machine is meant to be used repeatedly for a wide spectrum of its construction variants. Hence, it is useful to have an automatic or at least interactive editor of the model and of the analysis. This chapter defines the model and user interface requirements.

3.1.1 Model requirements

- **Saving and loading models** - the model should be able to be saved for future analysis or for analysis under different conditions.

- **Material library** - there should be an option to choose the material in *FEMM* or define a new material, including the possibility of a non-linear *B-H curve.*

- **Importing geometry** - the geometry of the stator and rotor is often available in *CAD* file formats and importing into *FEMM* is quite smooth, thus such importation is to be included in the editor.

- **Analysis setting** - since the analyzed area can differ from machine to machine there should be the ability to select geometry entities for computation of the desired quantities.

- **Simplified geometry ability** - the machines often have periodic shapes of stator and rotor cores and this fact can facilitate working with the model as well as shortening the performed analysis

3.1.2 User interface abilities

- **Visualization of geometry** - the user should be able to see the imported geometry, zoom or pan within the geometry in order to set appropriate properties of geometric entities.

- **Intuitive user interface for defining a new model** - the user should be able to define the required attributes of a new model

- **Intuitive user interface for defining analysis conditions** - the user should be able to define the required analysis conditions, i.e. number of iterations, range of varying quantity, etc.

- **Groups** - working with the geometric entities shall be facilitated by labeling them into groups.

4 Analysis of induction machine

Analysis deals with the design of each electromagnetic, electric and thermal model. All together, they form a *lumped-parameter model* (*LPM*). This work also deals with the implementation of each model in both *Matlab* and *FEMM*.

4.1 Structure of program

The program takes care of the model from its creation to evaluation of machine parameters. It consists of several programs, graphical-user-interfaces (*GUIs)* and functions written in *Matlab*.

4.1.1 Overall structure

Since it is possible to import the geometry into *FEMM* the *LPM* is based on *dxf* files that can be created in *CAD*. Materials and other properties are mainly set in *Matlab* in *config*.m file and via *New_GUI*, which is a graphical-user-interface for creating any new *FEMM* model. However, several optional properties existing in *FEMM* can be modified directly by editing them through a *FEMM* window. In figure 4.1, it is obvious that *FEMM* is used as a *grey box* with some inputs and outputs in the *LPM*.
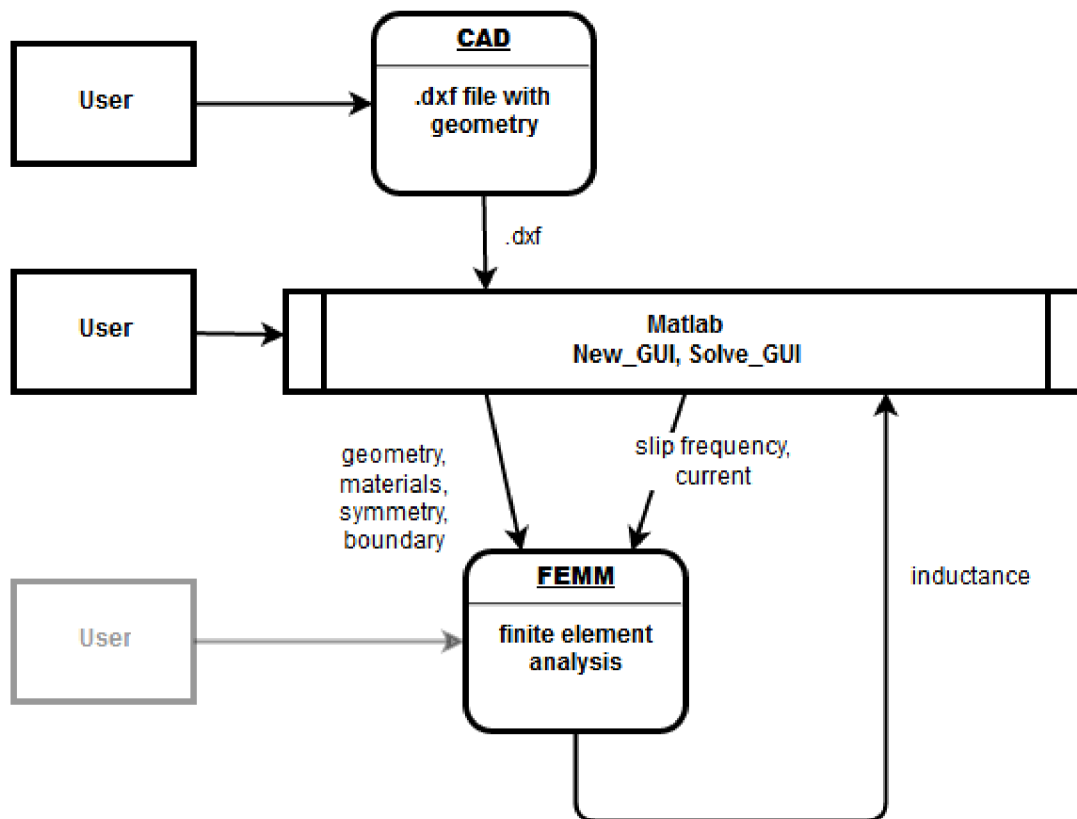

Figure 4.1: Software connections

Each file that contains the *LPM* is stored in two parts – a *.fem* sub-file used by *FEMM* and a *.mat* sub-file used by *Matlab* that contains important information about the other physical attributes of the machine.

4.1.2   Defining a new model

The shape of the machine does not vary during all simulations, however, some properties of blocks are to be changed and/or measured. For this reason it is necessary to define and store their labels and values. All enclosures of the *2D FEMM* model must have predefined block properties such as *x-y coordinates* of the label, *type of material*, *mesh size*, *group*, *name of electrical circuit*, *number of turns of the circuit* and more. There are also other properties that need to be set in *FEMM* such as *depth*, *precision*, *dimension units* and more, but they do not vary at all and thus they are held in the *config.m* file.
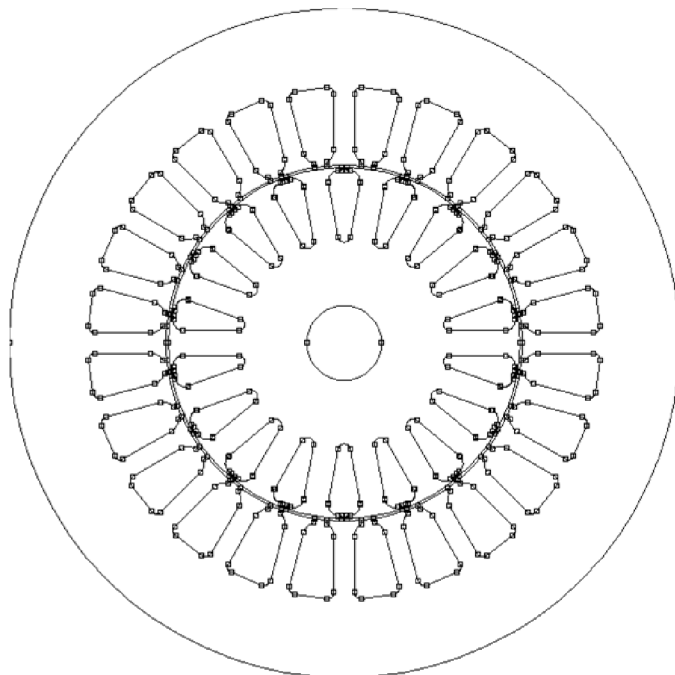

Figure 4.2: Imported geometry

A new model can be built using a *Main.m* file. When running this file, the code will automatically open both a new electromagnetics project in *FEMM* and a *New_GUI*. While the user creates the block labels one can see they are added to the opened *FEMM* project, immediately.
Working with block labels can be facilitated when they are in groups, especially in the case of the stator winding and rotor bars. *FEMM* enables assigning block labels to groups; nevertheless, in the case of importing geometry *FEMM* assigns some group numbers to different parts of the geometry. In order to avoid mismatches, an independent group system in *LPM* is developed.
The *New_GUI* shows the imported geometry (figure 4.2) while the user can add the block properties to the enclosures. The properties involve types of material which can be basically divided into three categories: predefined materials, user-defined materials and user-defined non-linear materials. The materials are held in *config.m* file in a library of materials. The predefined materials are variables of type *string* with the name of material that is identical to the name of material in the *FEMM* library. The user-defined materials are variables of type *row vector* and it follows the sequence of quantities used in *mi_addmaterial* function which is described in [12]. The user-defined non-linear materials are defined in the same manner aside from the last quantity which is a matrix with pairs of *flux density B* and *magnetic field strength H*.

The *New_GUI* is also used for setting restricting physical boundaries in lines and arcs. An important property of stator winding slots is the number of wires and direction of current flow and thus it is defined in the *New_GUI* as well.

4.1.3   Defining conditions for analysis

A *Solve_GUI* file has been created in *Matlab* for setting analysis parameters. Using this *GUI* the user can define the range of slip frequencies, maximum count of iterations, stop-criterion of iterations, desired output power, and some selections of block labels for subsequent integrations which are furthered by *FEMM* postprocessor. At this point for example, it is useful to have the rotor parts in a group because the generated torque is integrated for the whole rotor in the *FEMM* postprocessor.

4.1.4   FEMM interface

The *LPM* communicates with *FEMM* through the *Octave-FEMM* interface. The full list of commands is presented in paper [12]. A few of them are implemented in the LPM. It is useful to know that the commands can be divided into three types: system, preprocessor and postprocessor commands. System commands are used to maintain the *FEMM* files, adjusting screen size, saving bitmaps, etc. Preprocessor commands have prefix *mi_* which stands for magnetics-input. These commands are used to adjust model parameters during the creation and simulation of machine models. Finally the postprocessor commands have prefix *mo_* which stands for magnetics-output. These are used for reading physical quantities from the analyzed *FEMM* model.

4.2 Electromagnetic model

Electromagnetic modeling is performed through *FEMM* with *Matlab* as a companion. *Matlab* adjusts the properties of the *FEMM* model, then *FEMM* computes the finite element analysis of the induction machine configuration and *Matlab* obtains specific resulting values of flux and torque. Subsequently the induction parameters are derived using the *least-square-fit*.

4.2.1   Gathering the flux and torque

Flux can be obtained after analyzing the model in *FEMM*. At first, the circuits must be defined. A property named *circuit* can be added to a block label in the *New_GUI*. The configuration given to *FEMM* depends on the number of slots, the number of phases that occur in the machine and the number of poles of the machine as well. A quick example is found in figure 4.3.
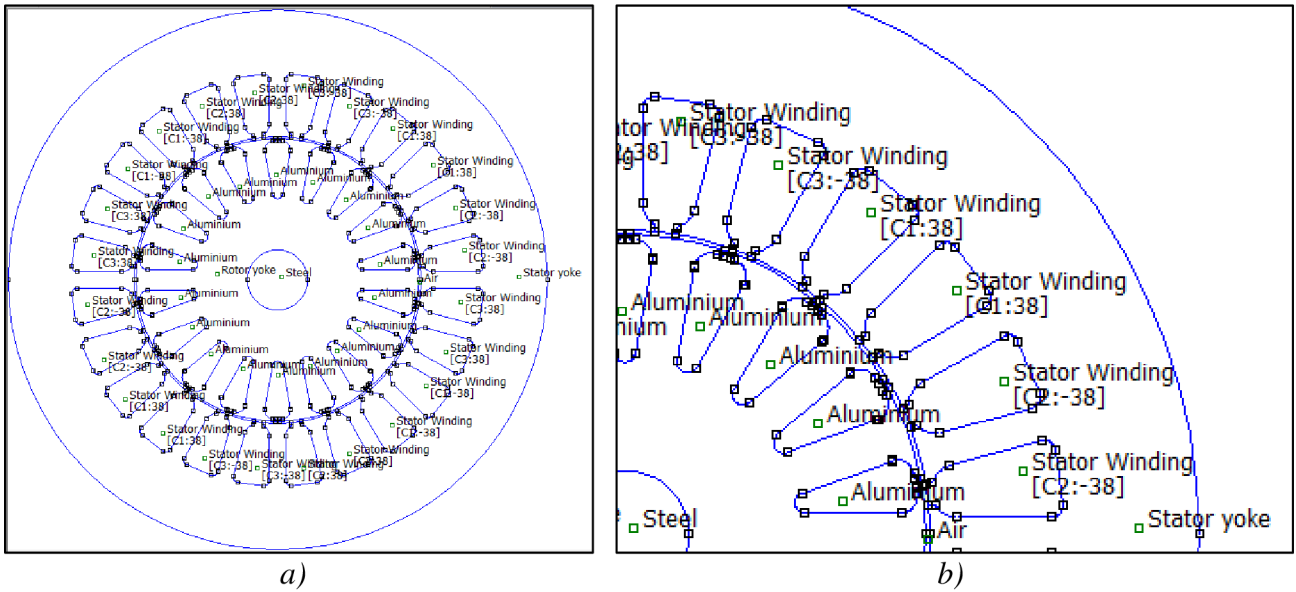
a)   b)

Figure 4.3: a) Defined new *FEMM* model and b) Closer view of the circuits

This example deals with a *three-phase four-pole* machine and thus it needs at least three circuits. In the case of a three-phase power supply, each phase is *120°* delayed after the previous and *120°* before the next. This issue is expressed as a complex value of the current flowing in the circuit. For our purposes the current amplitude of each phase is equal and therefore we can use exactly one value of amplitude for all phases. The current will be automatically transformed into a complex value using the *importCrrnt* function. Assuming a *current* flowing through the first phase, the second will have a value according to:

$$current_{+120°} = -\frac{current}{2} + i \cdot \sqrt{\left(current^2 - \left(\frac{current}{2}\right)^2\right)} =$$
$$= current \cdot \left(-\frac{1}{2} + i \cdot \frac{\sqrt{3}}{2}\right)$$

(4.1)

When the *current* has value *1A* we obtain the complex value above in the brackets for the delayed second phase (equation 4.1). One can notice that for the third phase the complex value is a complex conjugate. However, these complex numbers are different at different n-phase configurations and the derived rate in equation 4.1 is valid only for *120°* delayed phase configuration (three-phase). Another property of stator winding is the number of turns linking the current inside of each slot. In figure 4.3 we can see the stator winding has additional information, for example *C2:-38*. *C2* is just a name for the second circuit but the *-38* is more interesting. The reader may intuitively guess that the number truly is a count of turns of winding in the slot. The minus is here because there are two different directions of the wire which either enters or exits the slot. That means the wires in the opposite slot of the same circuit must have the opposite direction upon entering the slot.

Analysis of electromagnetic quantities is started via *Matlab* using the *mi_analyze* function. When this semi-solution is completed the properties of circuits can be evaluated. The function *mo_getcircuitproperties* gives us a value of flux linkage caused by the selected circuit.

The torque can be computed via a function written in *Matlab* named *femIntegrate*. This function is based on the *mo_blockintegral* function that can integrate various physical quantities of chosen blocks. In the case of generated torque the user needs to choose all parts of the rotor. In this case, the integrated area must not have holes in it. Therefore, input of the *femIntegrate* function has to involve all blocks inside of the rotor even when filled with air or another coolant.

4.2.2 Deriving machine parameters

The aim is now to express how the machine will react upon varying outer conditions. Consequently, we need to calculate the parameters which are described in section 2.1.2. When we use the linearization of the *B-H* curve mentioned in section 2.2.1 the parameters are almost independent on both the slip frequency and current and thus the approach, described in 2.3.2, can be used. Next, for a range of slip frequencies we can acquire an approximation of these machine parameters. For each *slip frequency* f_s we get matching *flux linkage* Φ which is a complex value. Provided the current amplitude is the same in each frequency f_s we can divide the overall flux with the current amplitude and get *phase-inductance* $L(f_s)$ matching to the frequency.

According to section 2.3.2 we can formulate equation 2.22 inversely and get M, τ and L_l using the *least-square-fit method*. We need a rotational speed

$$\overline{\omega_s} = 2\pi \overline{f_s} \tag{4.2}$$

where $\overline{\omega_s}$ is a column vector of analyzed *slip frequency* in rad/s. Then when we define a matrix $k \times 2$

$$\boldsymbol{m} = \begin{bmatrix} \omega_{s,1} & \omega_{s,1}{}^2 \cdot L_{i,1} \\ \vdots & \vdots \\ \omega_{s,k} & \omega_{s,k}{}^2 \cdot L_{i,k} \end{bmatrix} \tag{4.3}$$

where $\overline{L_i}$ is a column vector of the imaginary part of the complex inductance mentioned above. And then we transpose the matrix

$$\boldsymbol{A} = \boldsymbol{m}^T \tag{4.4}$$

And when we define an opposite inductance

$$\overline{b} = -\overline{L_i} \tag{4.5}$$

We can now do the *least-square-fit* and obtain the coefficients

$$\begin{bmatrix} c_1 \\ c_2 \end{bmatrix} = (\boldsymbol{A} \cdot \boldsymbol{m}) \backslash \boldsymbol{A} \cdot \overline{b} \tag{4.6}$$

Then τ is a square root of the second coefficient

$$\tau = \sqrt{c_2} \tag{4.7}$$

And M is a fraction of the first coefficient

$$M = \frac{c_1}{\tau} \tag{4.8}$$

In the case of *leakage inductance* it is sufficient to use the mean instead of the *least-square-fit*. For $\overline{L_l}$ vector we get

$$\overline{L_l} = \begin{bmatrix} L_{r,1} - \dfrac{M}{1 - \left(\tau \cdot \omega_{s,1}\right)^2} \\ \vdots \\ L_{r,k} - \dfrac{M}{1 - \left(\tau \cdot \omega_{s,k}\right)^2} \end{bmatrix} \tag{4.9}$$

Finally for L_l we get

$$L_l = mean(\overline{L_l}) \tag{4.10}$$

It is good to know the matrix syntax in *Matlab* offers a dot form of working with matrixes, i.e. it performs element-by-element computation, and thus there is no need for *for-loop*. When the parameters are defined the *rotor resistance R_r*, which is viewed from the stator, can be expressed as

$$R_r = \frac{M}{\tau} \tag{4.11}$$

The content of this section is programmed in *Matlab* in a function named *deriveParam*. The *least-square-fit* is shown in figure 4.4. The acquired data $\overline{L_l}$ are obtained from *FEMM* circuit properties via the postprocessor and they correspond to the range of *slip frequencies* which has been set for the analysis. The parameters are placed in equation 2.21 and the curve is shown in figure 4.4. The *least-square-fit* is hereby very highly precise.
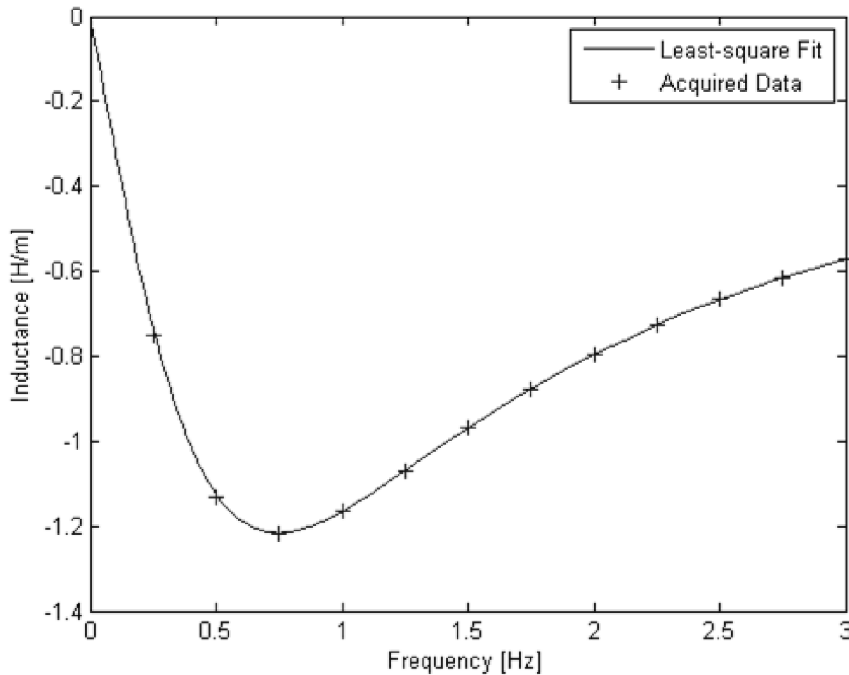

Figure 4.4: Graph of imaginary inductance per unit into-the-page over slip frequency

Consequently for torque, the *least-square-fit* is a little bit more deviated from the *acquired data* as shown in figure 4.5. The *acquired data* in this figure are also obtained via the *FEMM* postprocessor.
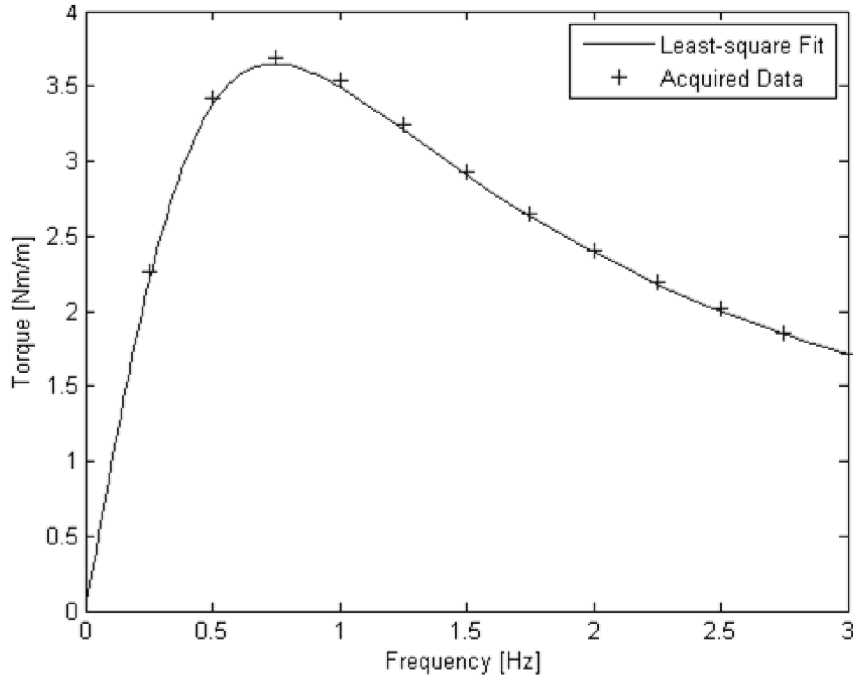
Figure 4.5: Graph of torque per unit into-the-page over slip frequency

The parameters, obtained using the *least-square-fit*, are placed in equation 2.7 whereby the torque curve is computed. The step-by-step computation of torque is described in section 4.2.3.

4.2.3   Operating point

Once the parameters of machine are determined we can predict its relations over slip frequency. All parameters in impedance equation 2.5 are known; thus, the *stator-phase-current* can be evaluated:

$$I_s(\omega_s) = \frac{V}{Z(\omega_s)} \tag{4.12}$$

where V is an *RMS phase-voltage* and Z is a complex value of impedance. For the electrical power we need the real part of power of all three phases:

$$P_{el}(\omega_s) = 3 \cdot I_{s,r}(\omega_s) \cdot V \tag{4.13}$$

where the $I_{s,r}$ is a real part of the *stator-phase-current* obtained in 4.12. The mechanical power can be computed using *torque*. The *torque*, generated by all phases, is with respect to equation 2.7 dependent on the *rotor current*. Having the impedance derived in equation 2.5 and the value of *RMS phase-voltage*, the rotor current can be derived with an almost identical procedure as in section 4.3.1 for nonlinear analysis. Subsequently, the *torque* is expressed as

$$T(\omega_s) = 3 \cdot p \cdot M \cdot \left(I_s(\omega_s)\right)^2 \cdot \frac{\tau \cdot \omega_s}{1 + (\tau \cdot \omega_s)^2} \tag{4.14}$$

Then the *output power* P_{mech} can be expressed as

$$P_{mech} = T \cdot \omega_{mech} \tag{4.15}$$

where the *mechanical rotational speed* ω_{mech} can be expressed as

$$\omega_{mech} = \frac{\omega - \omega_s}{p} \tag{4.16}$$

Finally the *output power* in relation to the slip frequency is

$$P_{mech}(\omega_s) = T(\omega_s) \cdot \frac{\omega - \omega_s}{p} \tag{4.17}$$

When the *output power* is determined the *efficiency* of the machine can also be calculated. Considering an ideal machine having only stator-winding and rotor-winding losses, the *efficiency* is

$$eff(\omega_s) = \frac{P_{mech}(\omega_s)}{P_{el}(\omega_s)} \tag{4.18}$$

We could also derive the rate of how much electricity is consumed by effective resistances

$$\cos\varphi\,(\omega_s) = \frac{I_{s,r}(\omega_s)}{I_s(\omega_s)} \tag{4.19}$$

4.2.4   Nonlinear *B-H* curves

Mostly, the magnetic flux reaches saturation in both the stator and rotor teeth. In the case of linearization of the *B-H* relation, simulation is appropriate only till it reaches saturation. Otherwise, the results of the simulation are apparently better than they would be in a real machine. On the other hand, a simulation with the linearized *B-H* relation is several times quicker than the simulation with nonlinear relation. Thus, the linearization can be used for a snap-shot of machine capabilities. For example we can assume that the machine will not have a greater power on its shaft than in this simulation.

When the simulation with linearized *B-H* relation is done we can have a rough estimate of the operating slip frequency, the current flowing through the stator and subsequent values of quantities that occur in the machine. To simulate the machine with the nonlinear *B-H* relation, the user can copy the *fem* model with its matching *mat* file and modify it. If the model was created while having the nonlinear material in the *config.m* library one can simply open the copied *fem* model, then change a property of stator's and/or rotor's yoke block label with the desired nonlinear material. It is good to note that the *mat* file carries only positions of block labels and a few initial values and thus the material can be changed in addition, easily and without worries.

As the *flux* reaches saturation, the machine parameters become more dependent on the *current* that flows around the material. Also, the value of *rotor current* is dependent on the *slip frequency*. After all, the computed values of the parameters of machine depend on the actual value of *stator current* and the actual *slip frequency* as well. In fact, the stator current also depends on the *slip frequency*, thus the parameters can be assumed to be dependent on the *slip frequency* alone.

In order to specify the parameters accurately, the simulation is to be performed within a short range of *slip frequency* and a specific *current* flowing in the stator winding. In figure 4.6 we can see two situations of derived parameters of the same machine. In the first, the range of *slip frequency* is from *0.25* to *3 Hz* and in the second the range is from *2.97* to *3 Hz*. In both cases the simulated machine has a linear material and all other properties of simulation are the same. One could judge the shortened range is almost 1% longer than the longer one and the deflection is still small,

usually less than 1%. Assuming the machine parameters do not vary inside of the shortened range too much we can afford such approximation of machine parameters for the nonlinear *B-H* relation.
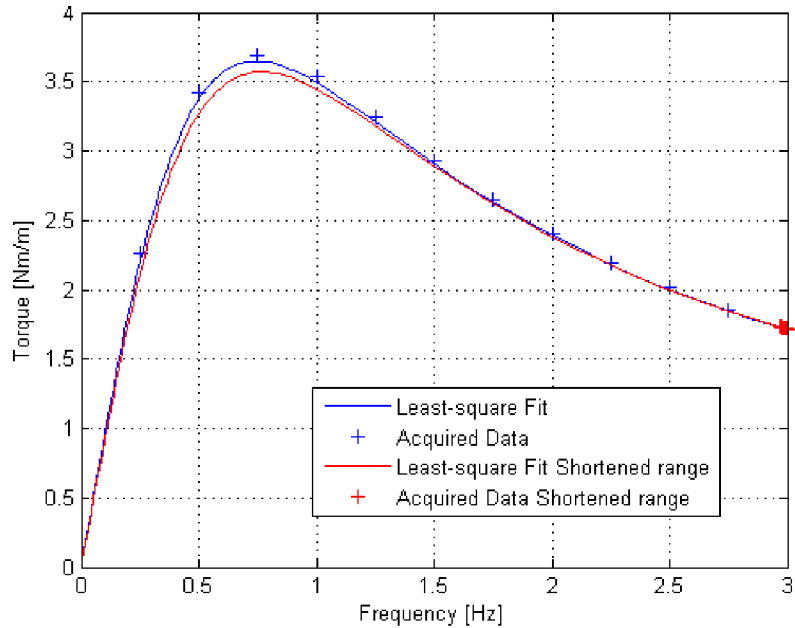

Figure 4.6: Shortened range of *slip frequency* effect

4.3 Electric model

Induction machines can be built in different construction shapes especially with different types of rotor cage. This work deals with a simple rotor cage with one layer topology. The designed electrical model describes the mentioned rotor configuration and for other types it can differ.

4.3.1 Modeling a simple rotor cage

Many induction machines have a 3-phase power supply. Each phase can be modeled using the electrical schema shown in figure 2.4. This schema works for materials with linear *B-H* relation. According to section 4.2.4 the parameters τ, M, L_l, R_r are no longer constant when using a non-linear material. The schema for an induction machine with non-linear materials is shown in figure 4.7.
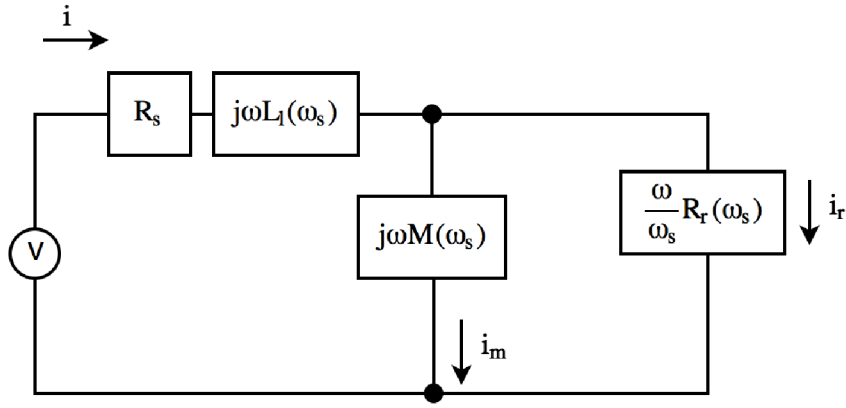
Figure 4.7: Electric schema with varying parameters

The parameters except R_s are dependent on the *slip frequency*. Thus for each slip frequency, the rate of a stator and rotor current is different. However, the *rotor current* can be derived with dependency on the *stator current*. *Stator current* can be expressed as

$$I_s(\omega_s) = \frac{U_{parallel}(\omega_s)}{Z_{parallel}(\omega_s)} \tag{4.20}$$

where $Z_{parallel}$ is the impedance of the parallel branch of the electric circuit expressed in equation 4.21.

$$Z_{parallel}(\omega_s) = \left| \frac{i \cdot \omega \cdot M(\omega_s) \cdot \frac{\omega}{\omega_s} \cdot R_r(\omega_s)}{i \cdot \omega \cdot M(\omega_s) + \frac{\omega}{\omega_s} \cdot R_r(\omega_s)} \right| \tag{4.21}$$

The *rotor current* can be expressed as

$$I_r(\omega_s) = \frac{U_{parallel}(\omega_s)}{\frac{\omega}{\omega_s} \cdot R_r(\omega_s)} \tag{4.22}$$

After replacing $U_{parallel}$ from equation 4.20 into 4.22 we get

$$I_r(\omega_s) = \frac{I_s(\omega_s)}{\left| 1 + \frac{R_r(\omega_s)}{i \cdot \omega_s \cdot M(\omega_s)} \right|} \tag{4.23}$$

And finally assuming $\tau = M/R_r$ we obtain

$$I_r(\omega_s) = I_s(\omega_s) \cdot \left| \frac{i \cdot \omega_s \cdot \tau(\omega_s)}{1 + i \cdot \omega_s \cdot \tau(\omega_s)} \right| \tag{4.24}$$

which is valid when $\omega_s \geq 0$. Analogously the magnetizing current could be derived.

4.3.2 *Wye* or *delta* connection

One important thing about *n-phase* connections is the mutual connection between phases. *3-phase* machines are usually connected as either *wye* or *delta*. The difference between them is in relation of the phase and line quantities. In both cases we need to know the exact voltage applied on a phase. With the *delta* connection, the *phase voltage* is equal to the *line-to-line voltage* but the *phase current* is lower than the *line current*. With a *wye* connection, the *phase voltage* is lower than the *line-to-line voltage* but the *phase current* is equal to the *line current*. The *phase current* is the quantity required for the electrical schema in figure 2.4 and 4.7 that is derived for one phase. The *line-to-line voltage* can be expressed as

$$V_{Y,line-to-line} = \sqrt{3} \cdot V_{Y,phase} \tag{4.25}$$

for the *wye* connection and

$$V_{\Delta,line-to-line} = V_{\Delta,phase} \tag{4.26}$$

for the *delta* connection. The connections of phases are outlined in figure 4.8.
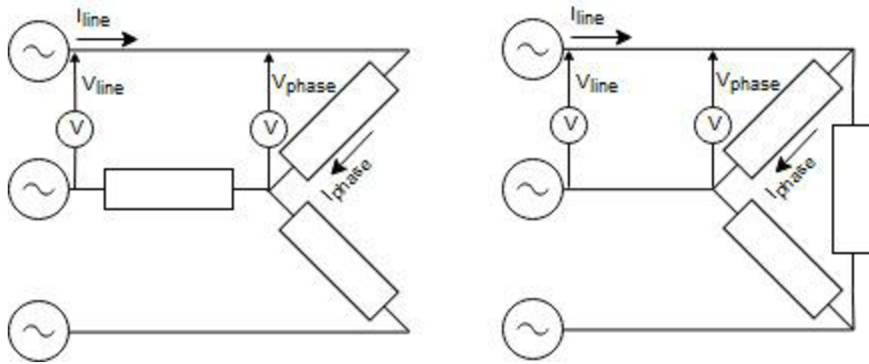

Figure 4.8: *Wye* and *delta* connection

4.3.3 Estimating resistances and inductances

The induction machine has several conductors with resistances and inductances. The inductances are computed via the *FEMM* analysis; however, this analysis is based also on the rotor's resistivity. The rotor consists of rotor bars and rotor end-rings. Even though *FEMM* works only in *2D* it is possible to adjust the conductivity of the rotor bar material in order to involve the rotor end-rings resistance. The *combined conductivity* of rotor material can be expressed as

$$\sigma_{combined} = \frac{1}{\rho_{combined}} \tag{4.27}$$

where $\rho_{combined}$ is a *combined resistivity* which can be expressed as

$$\rho_{combined} = R_{combined} \cdot \frac{S_{bar}}{l_{bar}} \tag{4.28}$$

where $R_{combined}$ is a *combined resistance*, S_{bar} is a *cross-section-area* of rotor bar and l_{bar} is the length of the bar. $R_{combined}$ is an addition of the rotor bar resistance with the end rings resistance as in equation 4.29.

$$R_{combined} = R_{bar} + 2 \cdot \frac{R_{ring}}{\Delta^2} \tag{4.29}$$

where Δ is a coefficient which involves the configuration of bars and poles. The coefficient is expressed in equation 4.30.

$$\Delta = 2 \cdot \sin\left(\frac{\pi \cdot p}{Q_2}\right) \tag{4.30}$$

The p is connected to a number of poles as mentioned in section 2.1.1 and Q_2 is the number of rotor bars as mentioned in section 2.1.5. R_{bar} is the resistance of one rotor bar and R_{ring} is the resistance of an arc segment between two bars (middle to middle). A similar approach is shown in [3]. One would note, that the Δ depends on the rate of number of poles and number of bars but not the number of phases. This fact can be observed in figure 4.9 wherein the *density of current* in rotor bars follows the contours of *magnetic flux* in the rotor.

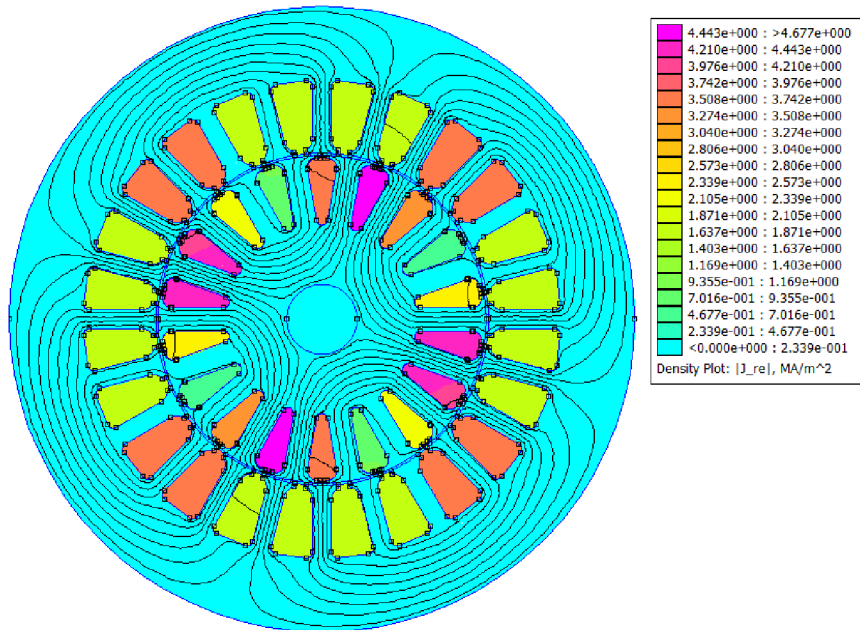| 4.443e+000 : >4.677e+000 |
| 4.210e+000 : 4.443e+000 |
| 3.976e+000 : 4.210e+000 |
| 3.742e+000 : 3.976e+000 |
| 3.508e+000 : 3.742e+000 |
| 3.274e+000 : 3.508e+000 |
| 3.040e+000 : 3.274e+000 |
| 2.806e+000 : 3.040e+000 |
| 2.573e+000 : 2.806e+000 |
| 2.339e+000 : 2.573e+000 |
| 2.105e+000 : 2.339e+000 |
| 1.871e+000 : 2.105e+000 |
| 1.637e+000 : 1.871e+000 |
| 1.403e+000 : 1.637e+000 |
| 1.169e+000 : 1.403e+000 |
| 9.355e-001 : 1.169e+000 |
| 7.016e-001 : 9.355e-001 |
| 4.677e-001 : 7.016e-001 |
| 2.339e-001 : 4.677e-001 |
| <0.000e+000 : 2.339e-001 |

Density Plot: |J_re|, MA/m^2

Figure 4.9: Density of real part of current, on-load simulation

Final *combined conductivity* of the rotor bar can be expressed via conductivity of material and the rotor's topology as

$$\sigma_{combined} = \sigma_r \cdot \frac{1}{1 \cdot k + 2 \cdot \frac{\pi \cdot D_{ring,m}}{\Delta^2 \cdot Q_2 \cdot S_{ring}} \cdot \frac{S_{bar}}{l_{bar}}} \tag{4.31}$$

where $D_{ring,m}$ is a mean diameter of the rotor end ring and S_{ring} is its *cross-section-area*. The k factor represents an increase of resistance due to *skin effect*, in other words, the fact that the current is flowing rather near the surface of a thick conductor than uniformly distributed through the whole

section. Nevertheless, the skin effect occurs when the frequency of the current is higher than in the case of a usual induction machine and *FEMM* also works for low frequency problems where the *skin effect* is negligible. For our purposes $k \approx 1$.

The stator phase resistance is required for analysis only in form of resistance instead of conductivity. Provided the wiring of the phase is serial connected, the *stator resistance* can be expressed as

$$R_s = \rho_s \cdot \frac{l_{phase}}{S_{phase}} \tag{4.32}$$

where the ρ_s is *resistivity of the stator wiring material*; the S_{phase} is the cross section of one wire; and the l_{phase} is the length of all wires in the phase. This length depends on the configuration of wires inside of the induction machine including the end-windings. Literature [3] deals with estimating the length of the wiring using empiric relations with dependency on core depth, the mean diameter of slots, type of insulation, the number of poles, etc.

4.4 Thermal model

Since there are a lot of types and shapes of induction machines it is useful to have at least a general approach to analyzing the heat flow through each part of the machine. In this work the thermal model is applied on a simple induction machine with air cooling around the casing.

4.4.1 Thermal net of electric machine

The machine topology can be split into several segments. In figure 4.10 we can see how these parts are split into segments depending on how they are constructed and how they are mutually connected. The whole machine can be divided into a shaft (grey), rotor (orange), stator (red) and casing (blue) in radial section. The white space inside and outside of the machine is air which is a fluid substance.
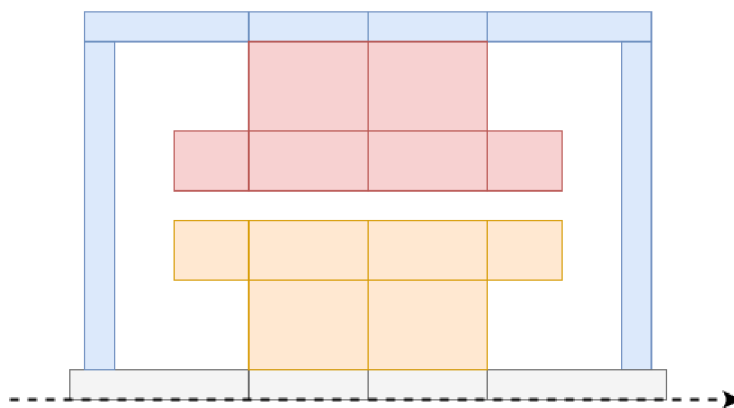

Figure 4.10: Radial section of machine topology divided into segments

As the topology is known the thermal net can be defined. Each segment can be represented as a node in the proposed thermal net. Specific position of the node in segment is not fundamental; however, the node shall be surrounded by the same material and usually it is put in the center of mass. The thermal resistance between each node can be represented as a firm connection (a line) between these nodes. The constellation is shown in figure 4.11. There is also a purposely hidden

connection between the air and nodes because the constellation in this figure shows only conduction; otherwise, the figure would be overcrowded with lines. Even though the convection is not showed in the figure the model has to involve it because it is substantial. In this case, each node is connected to outer and/or inner air which can also be separated into several segments.

One important issue, which cannot be viewed in a radial section of the machine, is the connection between the slot with electric conductors and the teeth of both the stator and the rotor. This issue can be seen in figure 4.3 *b)*. Hence, there are some extra nodes (5, 6, 15, and 16) that represent the teeth connected in a parallel way. Nodes 1 and 4 represent the stator winding end-faces. Analogously node 11 and 14 represent the rotor rings.
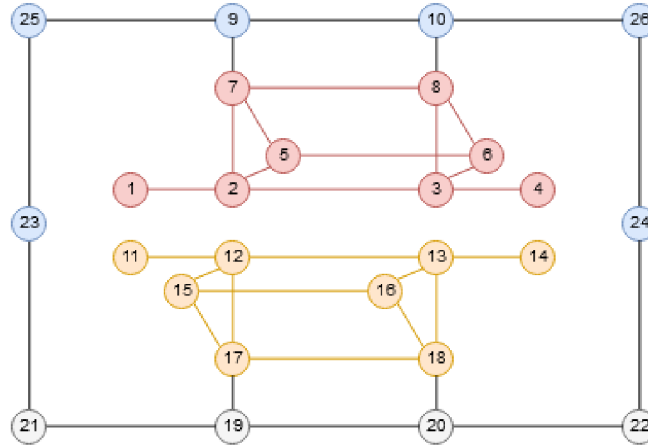
Figure 4.11: Thermal conductivity net of radial section of a machine

The accuracy of the thermal model is dependent on both a segmentation of the topology and estimation of the mutual resistances. These resistances are derived using the knowledge of heat transfer in section 2.4.1. For example the mutual resistance between nodes 7 and 9 consists of one *radial-thermal-contact* and two *radial-conduction resistances*, connected in series. Such resistance can be expressed as

$$R_{7,9} = \frac{1}{k_7} \cdot \frac{ln\left(r_{7,9}/r_7\right)}{2\pi \cdot L_{7,9}} + \frac{1}{h_{c,7,9} \cdot 2\pi \cdot L_c \cdot r_c} + \frac{1}{k_9} \cdot \frac{ln\left(r_9/r_{7,9}\right)}{2\pi \cdot L_{9,7}} \tag{4.33}$$

where k_7 and k_9 are a *thermal conductivity factor* of segment material ; $L_{7,9}$, L_c and $L_{9,7}$ are the length of segments in axial dimension; $r_{7,9}$ is a radius of boundary between segments; r_7 and r_9 are the radius of node 7 and 9; $h_{c,7,9}$ is the *thermal contact conductance*; r_c is the radius of the contact between segments.

The hidden resistance connected to air can also be derived. For example, the resistance between node 9 and the outer air (ambient) consists of *radial-conduct* and *radial-convection resistances* and can be expressed as

$$R_{9,amb} = \frac{1}{k_9} \cdot \frac{ln\left(r_{9,amb}/r_9\right)}{2\pi \cdot L_{9,amb}} + \frac{1}{h_{9,amb} \cdot 2\pi \cdot r_{9,amb} \cdot L_{9,amb}} \tag{4.34}$$

where $r_{9,amb}$ is the radius of the contact between the material and air (*ambient*); $L_{9,amb}$ is the length of segment in axial dimension; $h_{9,amb}$ is the *convection heat transfer coefficient* specific for the interface between the outer air and the surface of the segment.

In the end, after estimating all resistances, we can have an *n-by-n* matrix with all mutual resistances, where n is the number of nodes.

$$\boldsymbol{R} = \begin{bmatrix} R_{11} & \cdots & R_{1n} \\ \vdots & \ddots & \vdots \\ R_{n1} & \cdots & R_{nn} \end{bmatrix} \tag{4.35}$$

The relation between the *resistance matrix* and a *vector of temperatures* can be expressed as

$$\boldsymbol{R} \cdot \bar{T} = \bar{b} \tag{4.36}$$

where $\bar{T}$ is a *vector of temperatures* of nodes and $\bar{b}$ is a *vector of outer heat flux*, which is expressed as

$$\bar{b} = \begin{bmatrix} q_1 + R_{1,amb} \cdot T_{amb} \\ \vdots \\ q_n + R_{n,amb} \cdot T_{amb} \end{bmatrix} \tag{4.37}$$

where q is the *heat flux generated by the segment* and $R \cdot T_{amb}$ is the *heat flux that flows into the segment from ambient*. The temperatures formed to vector $\bar{T}$ can be obtained via an inverted matrix of resistances in this way

$$\bar{T} = \boldsymbol{R}^{-1} \cdot \bar{b} \tag{4.38}$$

This can be done easily in *Matlab* using the *back-slash* syntax. The coefficients k, h_c and h are experimentally determined and depend on material, surface, fins, fluid properties, type of motion, etc. Since the difference between the machine and the ambient temperature is not substantial the radiation heat transfer has been neglected in this model.

4.5 Lumped-parameter model

LPM combines the above models all together. The aim is to handle the mutual influences between all models.

4.5.1 Main concept

The *LPM* can be represented as an iterative process. In figure 4.12 there is a diagram symbolizing connections between the models, in other words, a schema of the whole process. At first we need to assume the initial state of the machine. We need at least a rough estimation of the parameters of the machine in order to define the operating point; thus, the electromagnetic model using *FEMM* should be the first model used in *LPM*. We could also assume the machine parameters but an assumption of stator current and temperature of conductors can be done more easily than an assumption of inductances and time constant. Also, we need to set the desired output of the machine – either an output power or torque. Finally, we can optionally set a *stop-criterion* which can be a number of iterations and/or maximal error. The grey boxes represent the models whereas the electrical is used twice in order to have consistent electrical quantities. The output of each box is shown below. The execution of the process is described more in next section.
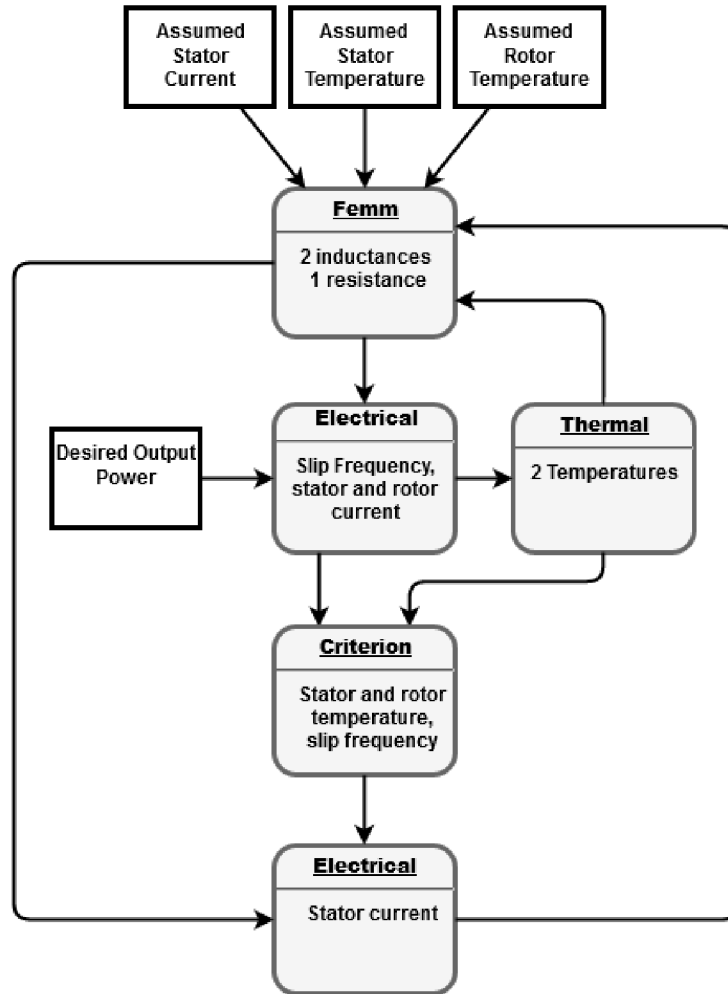
Figure 4.12: Lumped-parameter model

4.5.2   Connection between models

After the first assumptions we can calculate τ, M and L_l using the electromagnetic model, in figure 4.12 it is the box called *Femm*. Then we can use the electrical model and get a relation of machine quantities that depend on a slip frequency. Now, we can equal the derived relation of desired quantity with our desired value of quantity and solve this equation in order to get a specific slip frequency. In this paper we desire the output power. That means we equal the value of *desired output power* with equation 4.17 as in equation 4.39.

$$P_{mech}(\omega_s) - (P_{desired} + P_{mechloss}) = 0 \qquad (4.39)$$

$P_{mechloss}$ stands for *mechanical losses* due to friction in bearings and air friction, for example. We can use the *fzero* function in *Matlab* to solve this equation and find the specific slip frequency. A similar approach can be used when desiring the torque. Then the slip frequency can be used to compute the stator and rotor current using equations 4.20 and 4.24.

The thermal model requires a heat power dissipated in stator and rotor windings because they are the most significant heat sources. These *power losses of the stator* can be expressed for 3 phases as

$$P_{j,stator} = 3 \cdot (|I_s|)^2 \cdot R_s \qquad (4.40)$$

and for the rotor as

$$P_{j,rotor} = 3 \cdot (|I_r|)^2 \cdot R_r \tag{4.41}$$

Now the thermal model can be used for a calculation of temperatures in all nodes. If our assumptions were perfect the stator current and temperatures would be the same both before and after the process. Otherwise, we get a new state of the machine that differs from the previous one and we compare them. If the difference is smaller than the criterion we have sufficient results; otherwise the process must be repeated. Before repeating the process we must update the assumed quantities. Therefore, the electrical model is used again in order to get new electrical quantities adjusted to the temperature. The *resistance of the stator* in equation 4.32 can also be expressed in terms of a temperature as

$$R_s = R_{s20} \cdot (1 + \alpha_s \cdot \Delta T_s) \tag{4.42}$$

where R_{s20} is a *resistance of the stator* calculated with specific resistivity of the used material having a temperature of *20°C*; α_s is the *temperature coefficient of resistance* of the material; ΔT_s is the difference between the new temperature of the stator and the *20°* temperature. *FEMM* does not require the resistance of the stator because it only calculates with the current flowing through the stator winding; however, the stator resistance is essential in calculation of the current.

For the *combined conductance* of the rotor in equation 4.31 we can use a similar approach subjected to temperature increase.

$$\sigma_r = \sigma_{r20} \cdot \frac{1}{(1 + \alpha_r \cdot \Delta T_r)} \tag{4.43}$$

where σ_{r20} is the *conductance of the rotor* calculated with a specific conductivity of the used material having a *20°C* temperature; α_r is the *temperature coefficient of resistance* of the material; ΔT_r is the difference between the new temperature of the rotor and the *20°* temperature. This quantity needs to be updated in *FEMM*; therefore, the LPM uses the *mi_modifymaterial* function in order to update it.

The resistance R_r viewed from the stator winding, can also be adjusted to the new temperature. According to [3] the relation between the *real* and the *stator-viewed rotor resistance* for a simple rotor cage can be expressed as

$$R_r = R_{r,real} \cdot 4 \cdot m \cdot \frac{(N_1 \cdot k_w)^2}{Q_2} \tag{4.44}$$

where $R_{r,real}$ is the *real resistance of the rotor* derived in equation 4.29; m is the number of phases; N_1 is the number of turns in phase, k_w is the *winding fill factor* of stator winding and Q_2 is the number of rotor bars. We can see that the *stator-viewed rotor resistance* is directly proportional to *real resistance* and thus the influence of the temperature on it is the same as for other resistances. The stator-viewed rotor resistance can be expressed in terms of temperature as

$$R_{r,n+1} = R_{r,n} \cdot \left(1 + \alpha_r \cdot \left(T_{r,n+1} - T_{r,n}\right)\right) \tag{4.45}$$

where indexes n and $n + 1$ represent the number of steps in the iteration. In this case it is useful to calculate with a relative difference rather than the absolute. In other words, the resistivity is derived from the previous state.

The rotor resistance is connected to the time constant τ (equation 4.11). That means we can also adjust the *time constant* in the same manner

$$\tau_{n+1} = \frac{\tau_n}{\left(1 + \alpha_r \cdot \left(T_{r,n+1} - T_{r,n}\right)\right)} \tag{4.46}$$

Now we can use equation 4.12 and compute the phase current with adjusted resistances and the time constant. In order to update the stator current *Matlab* function *importCrrnt* has been created that imports the current into all phases using complex numbers as in section 4.2.1. It is important that the function calculates with an absolute value of the current, i.e. the amplitude of the current. We can use e.g. *abs* function in *Matlab* and transform it. Further, the function *importCrrnt* distributes the current into complex values matching to each phase as in section 4.2.1.

All the above dependencies on temperature are used with linearization of relation between electric resistivity and temperature. In most materials used for wiring in such machines it is sufficient to use this linearization.

4.5.3   Stability

The *LPM* is an iterative process that connects three models together. Each model is changeable; however, the basic rules do not vary. For example as the slip frequency gets higher the currents also get higher. Another example is that as the current gets higher the temperature also gets higher. High temperature causes higher electric resistance which restricts the current whereby the process is damped. In other words, if the machine can handle the desired torque or power the iterative process has a solution and it is convergent as the results proofed. Nevertheless, sometimes *LPM* can get oscillating. In that case, it is useful to involve some sort of damping in the process. It can be applied either to slip frequency or temperatures. It is analogous to a mechanical damping and it depends on the speed. The speed is expressed an increase of quantity per step. The damped quantity can be expressed as

$$x_{n+1,d} = x_{n+1} - d \cdot \frac{x_{n+1} - x_n}{(n + 1) - n} \tag{4.47}$$

where x is the quantity and d is the damping factor.

4.6 Tested machine

The model has been validated on a machine with a simple rotor cage. As a good sample, the *TM2-100-4L* has been chosen for its simplicity and availability. The results of the model are compared with those of another program called *EA100* as well as with the measured results of a real machine.

4.6.1   Input parameters of TM2-100-4L

At first it is required that we obtain the fundamental attributes of the machine. According to the data sheet, the machine has three phases and four poles. A further attribute that needs to be set is the geometry of the core. The programmed model enables the utilization of symmetries whereby the

computation in *FEMM* is shortened. Nevertheless, the machine can have splines, outer joints, holes and other unique factors and it is up to user to neglect them or not. The tested machine has one spline and one hole in the rotor plus six splines in the stator sheets. These components are neglected in this simulation and the machine geometry is simplified into one part of four which is shown in figure 4.13. Since the tested machine has four poles, we can split the geometry into four parts.
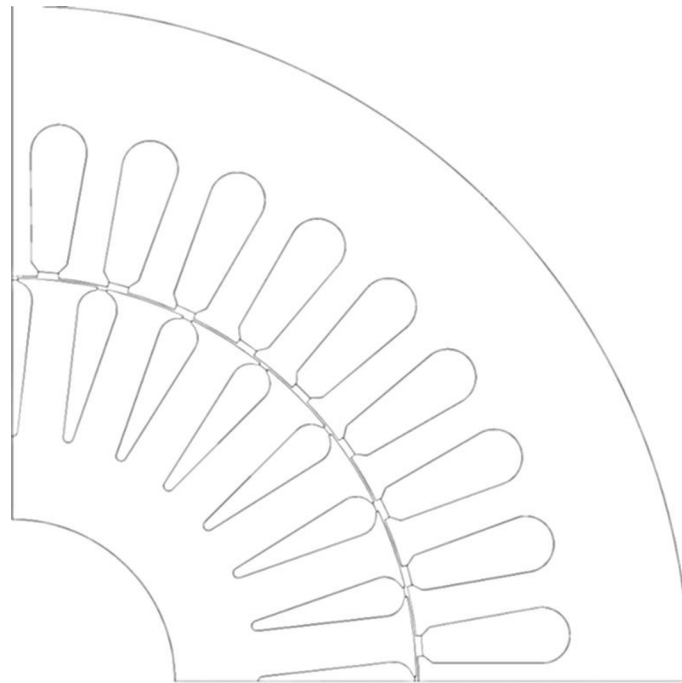

Figure 4.13: Simplified geometry of a machine

When using the symmetries, the analysis in *FEMM* is up to four times quicker. This simplification is possible only under some conditions. The neglected component must be far from the teeth and air gap; otherwise, it may have significant impact on its inductances. Also, the area must have whole slots for stator winding since the currents are flowing through whole coil slots. That means, the stator slot must not be cut in half as in the case of the rotor bar in figure 4.13. Another condition implies that all three phases must be situated exactly. We should note that the selected area produces one of four electromagnetic poles using exactly 9 stator slots. That means there are 3 slots for each phase located in a group. In case of some unique factors which are not symmetric according to the number of poles and which are significant, it would be difficult to analyze at zero speed. Additionally, it is required that the area is bounded, especially in the case of blocks located at the symmetry edge. One should note that the shaft is missing in the geometry. The shaft is intentionally neglected since it is made from steel which has low permeability and thus it hardly affects the magnetic flux at all. The geometry is designed in *AutoCAD 2012* and saved in a *dxf 2004* format. The depth of this *2D* geometry is set in the *config.m* file to *0.15m*.

Following attributes are the materials and their properties. All materials are held in *config.m* and one can easily work with them using *Matlab*. The air is a built-in material which does not need to be set. The rotor bars are made from aluminium. Its *combined conductivity* can be estimated using equation 4.31 depending on our predicted temperature of rotor bars according to the equation 4.43 as well. The *temperature coefficient of resistivity* of aluminium is equal to *0.0049/°C*. The *relative permeability* of this material is equal to 1. The next material is copper which is used in stator winding. This material is used in two cases. The first case is via *FEMM* when we need only its *relative permeability* which is equal to 1. The second case is when computing the *phase current*. In this case we need the resistance of all wires in one phase which can be computed using equation

4.32. The *phase resistance* is equal to 1.5171Ω and depends on temperature according to equation 4.42. The *temperature coefficient of resistivity* of copper is equal to *0.0068/°C*. The last material is iron in the stator and rotor sheets. The material is called *M470-50A* and its *B-H* relation is shown in figure 4.14 below.
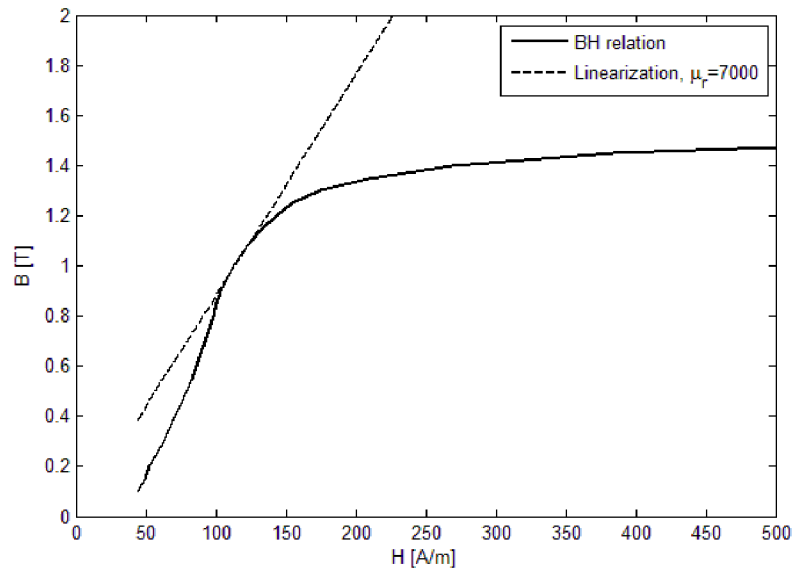

Figure 4.14: B-H relation of material M470-50A

The linearized *B-H* relation is set to *relative permeability* which equals *7000*. Both the real *B-H* curve and the linearized *relative permeability* are assigned in the *config.m* to a non-linear and a linear material respectively. Other properties of this material are its *conductivity* which is *0.2793 MS/m* and lamination. The *lamination thickness* is *0.5mm* and the *lamination fill factor* is *0.9*.

Another attribute of this machine is its power supply. It has *400V line-to-line voltage*, a *frequency of 50 Hz* and phases are *wye* connected. According to section 4.3.2, the *phase voltage* equals *230V*. The phase current is predicted as equaling *1A*.

Other important attributes are set via *GUIs*. The machine core configuration is shown in figure 4.15. We can see there are three circuits representing the phases with the number of turns and a sign which represents the direction of wires in the slot. Altogether, the configuration creates exactly one electromagnetic pole. There are also some hidden entities as boundaries which enclose the analyzed area. Four of them are axisymmetric that are used to connect the symmetry edges of the area. The last two are used to enclose the area at the shaft and at the outer surface of stator.
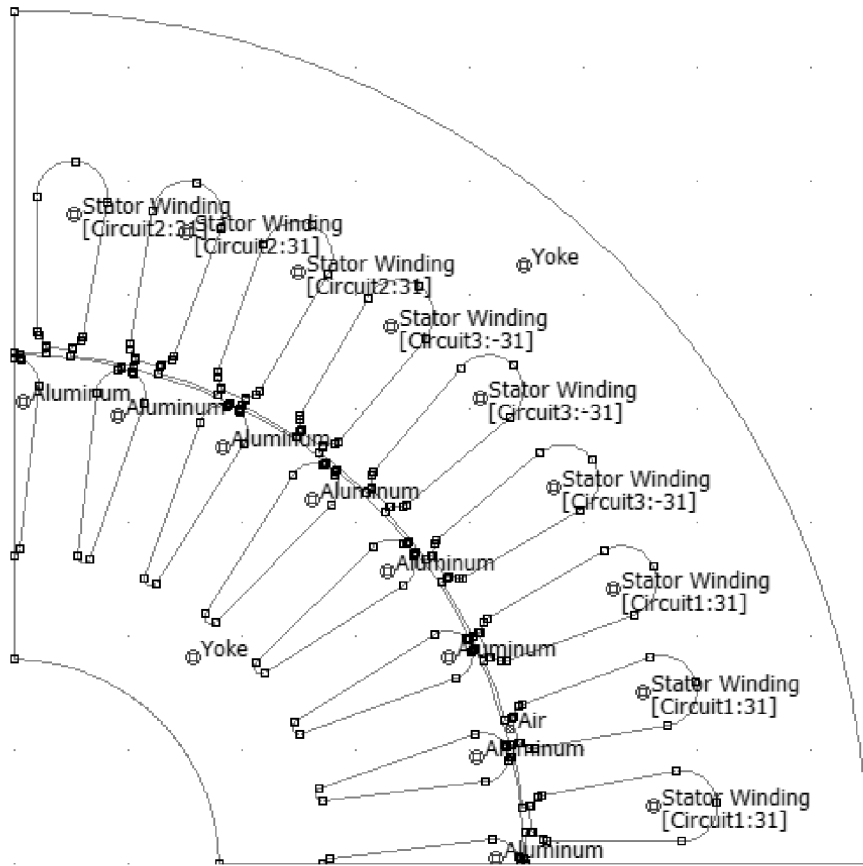
Figure 4.15: Core configuration

The thermal coefficients are held in the thermal model as well as dimensions of the casing and the inner parts. The joule losses dissipated in conductors are derived from the currents but it is required to separate them into segments in the thermal model. Also, the other losses must be estimated and assigned to the proper segments. This model considers *rotor teeth losses* to be equal to *1%* of the output power, *rotor yoke losses* to be equal to *0.5%* of the output power, *stator teeth losses* to be equal to *1.5%* of the output power and *stator yoke losses* to be equal to *1.5%* of the output power. The *mechanical losses* are expected to be *30W* and some *additional losses* to be *50W*. These expected losses are estimated for the machine approximately at operating speed, roughly at the nominal speed. In the electric model, all these extra losses are unified into the mechanical losses. The estimation of these losses is based on their usual behavior and it can be specified further.

4.6.2 Lumped-parameter analysis

Once the input parameters are defined we can define the conditions of the analysis. Considering the linear material, the range of slip frequency is set from *0.5* to *3Hz* with a step of *0.5 Hz*. The maximum number of iterations is set to be 10 and the stop criterion is set to be *<5°C* for stator and rotor temperature and *<0.5Hz* for the slip frequency. For each operating point the quantities differ. We can use *LPM* and compute the quantities for a range of output power. In other words, *LPM* is used several times for several operating points in order to compare it with the measured results.

A sample of one operating point, analyzed with *LPM* for *4500W* of desired output power, is now to be investigated. The analysis with linear material resulted in *slip frequency f_s = 4.75Hz* wherein the machine reaches the *desired output power*. This *slip frequency* can now be used for the analysis with non-linear material as a *reference slip frequency*. The analysis is performed with a slip

frequency range equal to $f_s \pm 0.03Hz$, i.e. from 4.72 to 4.78Hz. The analysis with non-linear material is repeated and results in slip frequency $f_s = 4.8Hz$ which does not lie within the used range. Thus, the analysis is performed once again and results roughly at $f_s = 4.8Hz$. The analysis is shown in figures 4.16, 4.17 and 4.18. In figure 4.16 a trend of *imaginary inductance L_i* through three iterations of the analysis can be seen. Curve number 1 with peak value at roughly *-0.9H/m* corresponds to the assumed input parameters of the machine, i.e. a temperature of *20°C* and stator current *1A*. Curve numbers 2 and 3 correspond to subsequent iterations. One thing to note is the fact that the criterion stated that the temperature must not be higher than *5°C* which has been satisfied after three iterations for non-linear material. In the case of linear material, the number of required iterations was only two including the initial iteration with assumed quantities.
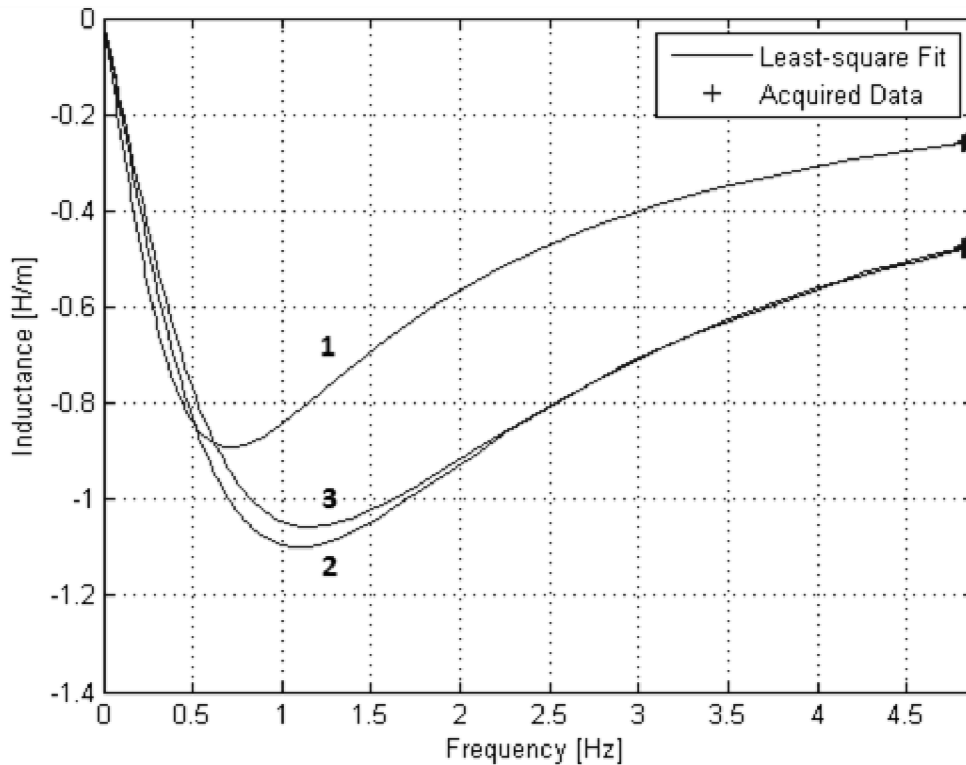
Figure 4.16: Inductance per unit into-the-page over slip frequency trend for *non-linear LPM*

The trend of torque over slip frequency is shown in figure 4.17. Regarding the torque it is important to note the fact that within one iteration exactly one stator current is entered into the model. Hence the torque shown here is related to one constant current over slip frequency and therefore it is totally different from the real relation between generated torque and slip frequency of the machine. We can also observe that the torque is much lower for the *1A* stator current and cool machine in the first iteration than in the case of the other iterations.
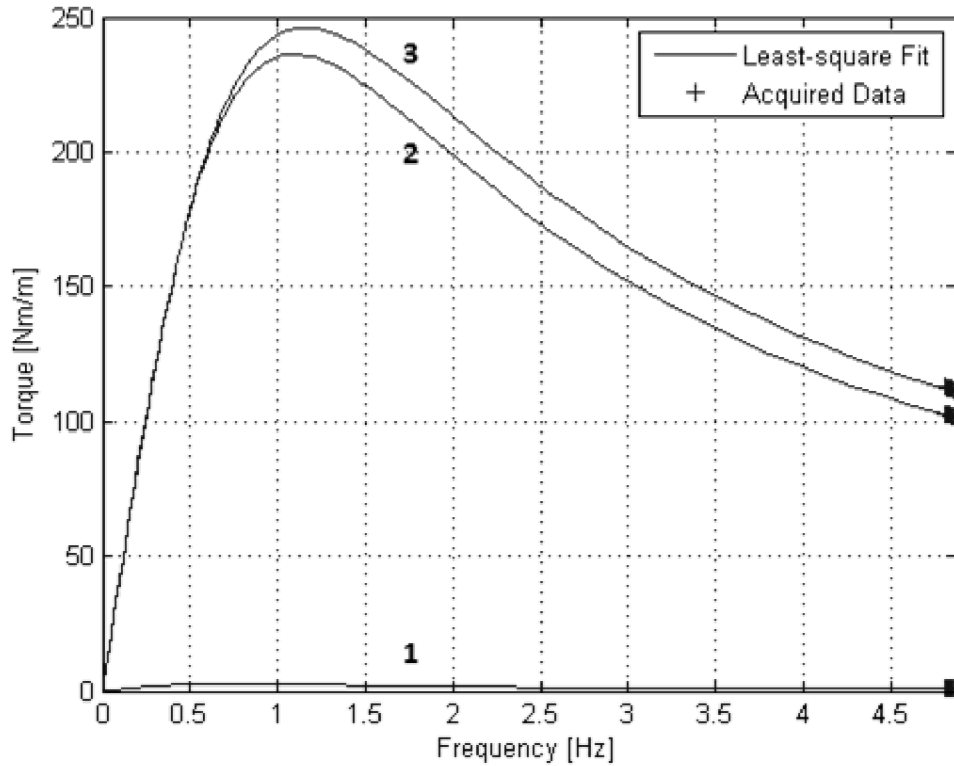
Figure 4.17: Torque per unit into-the-page over slip frequency trend for *non-linear LPM*

In the case of generated power in figure 4.18, the cool machine (assumed to be *20 °C*) generates significantly more power than when the machine is hot. The red line represents *desired output power* with added *mechanical losses*. The generated power equals zero when the slip frequency $\omega_s = 0\,rad/s$ or $\omega_s = 2\pi \cdot 50Hz$, which is the frequency of the power supply.
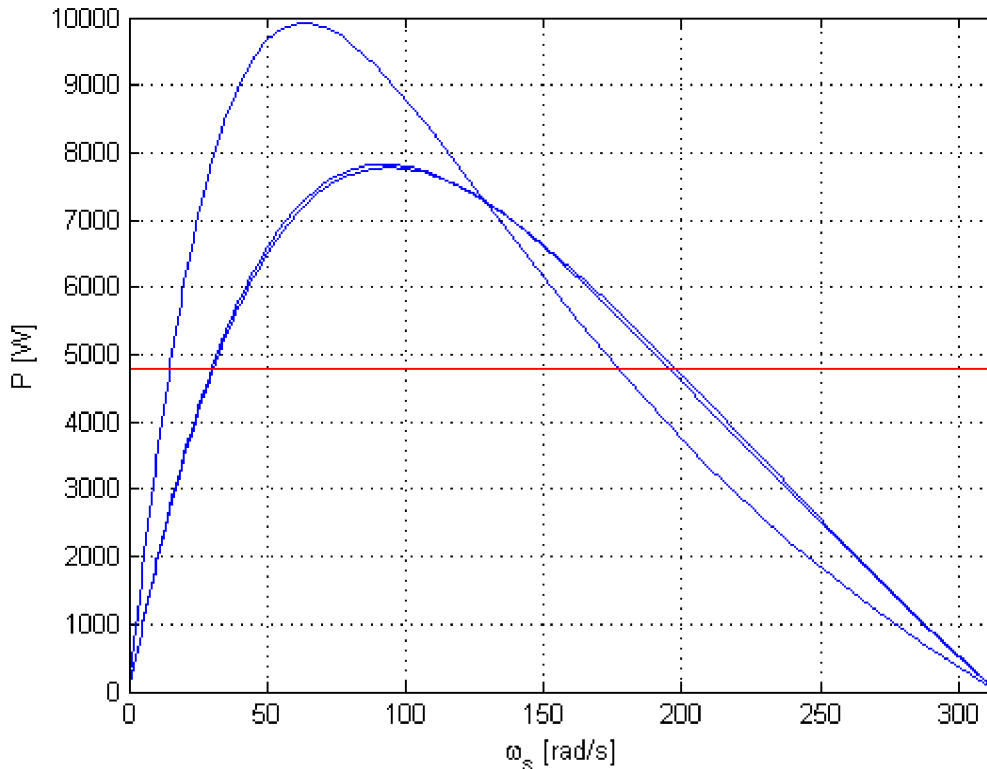
Figure 4.18: Power over slip frequency (angular speed) trend for *non-linear LPM*

4.6.3   Comparison of results

The machine was analyzed using the *LPM* for six operating points. The desired output powers were *500, 1000, 2000, 3000, 4000* and *4500 W*. Based on the analysis with linear material the next analysis with non-linear was also performed. The results of specific quantities were compared with the other computed by the analytical program *EA100* as well as with measured quantities of the machine at non-steady-state and steady-state after 12 hours of work. In fact, the steady-state is a thermal steady-state of the machine at nominal speed and torque because the measurement was performed within five minutes. Figure 4.19 shows the torque over slip frequency. We can see that the analysis was a little optimistic but in line with some oversight in the model we would expect this deviation.
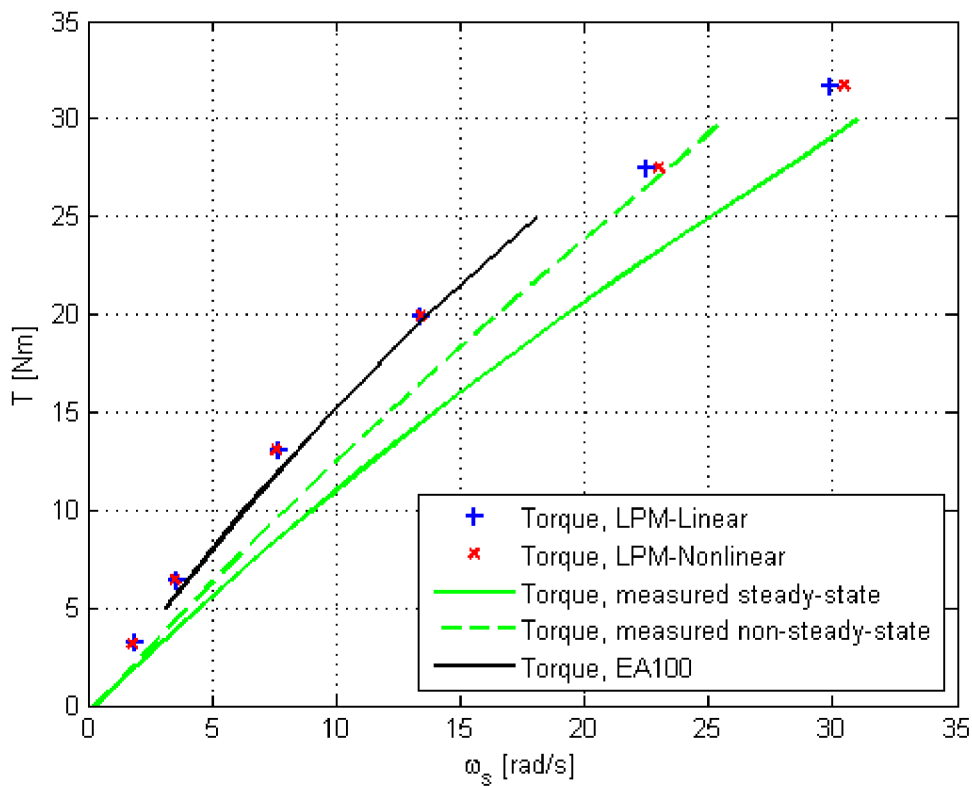
Figure 4.19: Comparison of torque over slip frequency (angular speed)

When we focus on the slip frequency of the same values of output power in figure 4.20 we can see differences between *linear* and *non-linear LMP*, especially when the power is more than *3000W*. The same value is reached in greater slip frequency for non-linear material. This fact is due to lower inductance caused by the flux saturation in the cores. An example of saturation is shown in figure 4.24. Also, there is a difference between the measured values for the steady-state and non-steady-state of the machine. In the case of the steady-state of the machine, the same output power is reached at higher slip frequency. This difference is caused by the temperature rise.
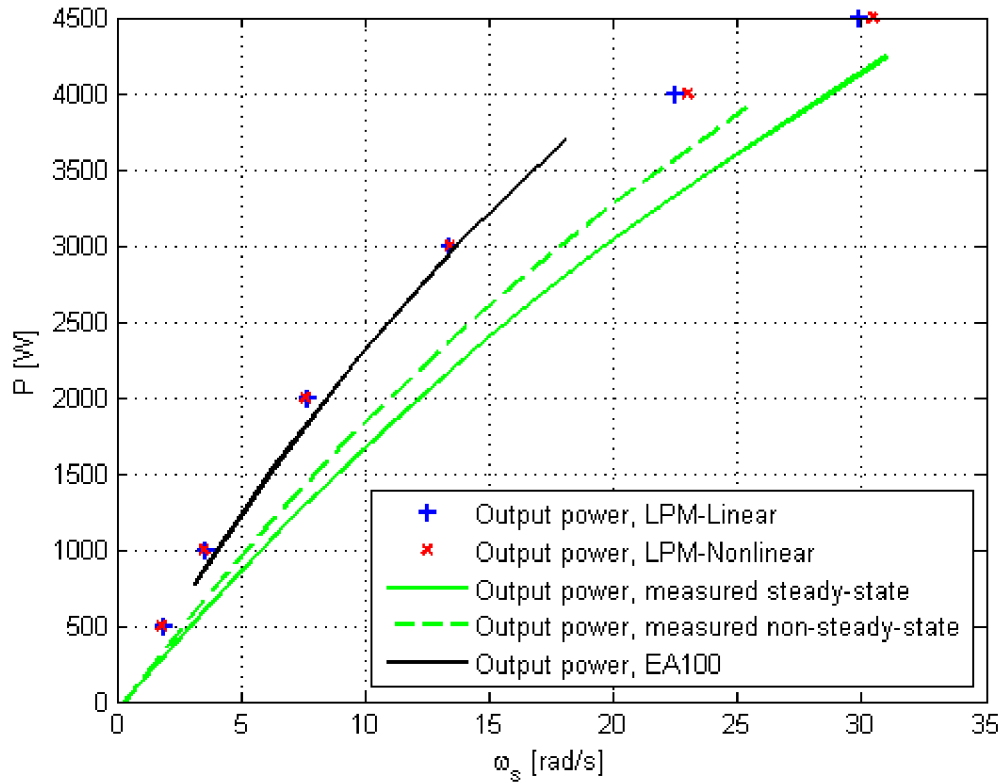
Figure 4.20: Comparison of output power over slip frequency (angular speed)

The resulted stator current in figure 4.21 is close to the real current at the nominal operating point wherein the desired output power is *3000W*. Although behavior near the zero slip frequency really differs. This issue is probably caused by the fact that the estimation of losses was defined mostly for a nominal operating state.

As in the case of the resulted current at a slip frequency close to zero, the efficiency in figure 4.22 differs as well. Nevertheless, at the nominal operating point with 3000W of output power the efficiency is a little bit closer to the real efficiency than with analytical method *EA100*.
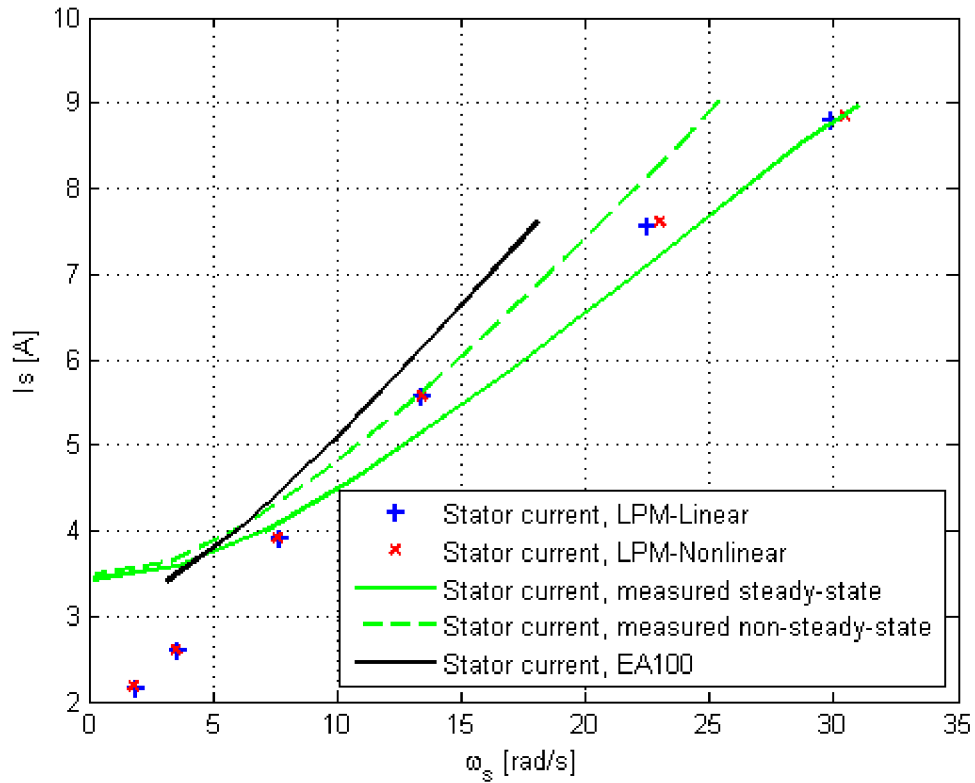
Figure 4.21: Comparison of stator current over slip frequency (angular speed)
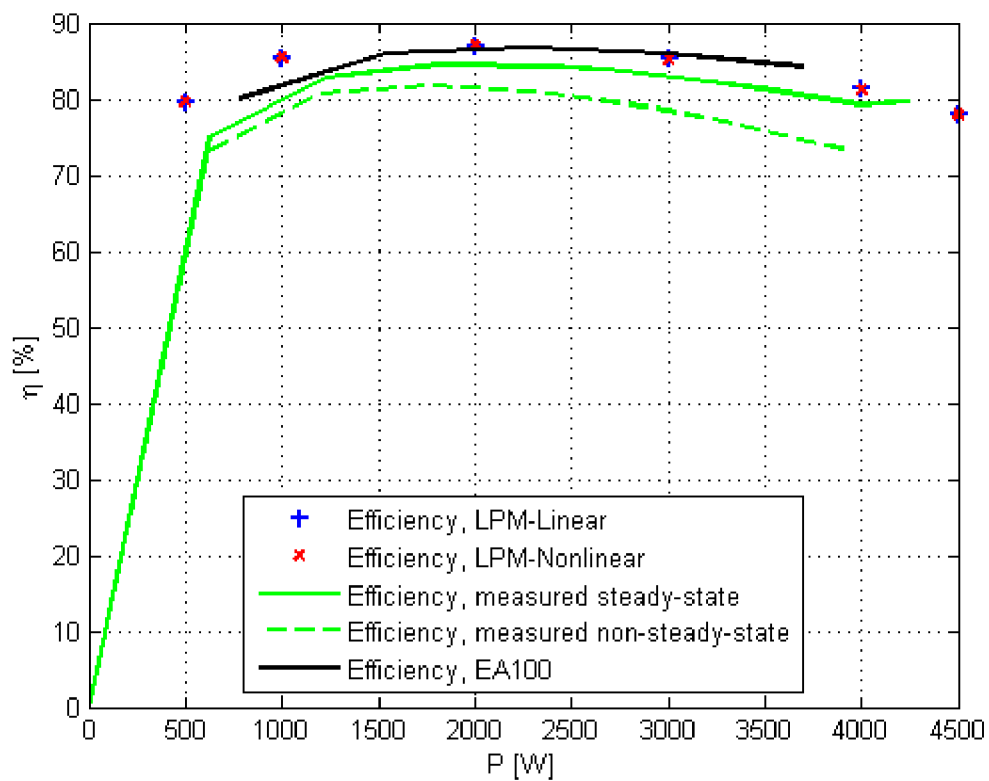
Figure 4.22: Comparison of efficiency over output power

In comparison of temperatures of the stator winding and rotor bars in figure 4.23 we can only assume the correct temperatures since the machine does not have temperature sensors. Beyond this, we can see that there is a difference between analytical method *EA100* and the *LPM* method. The *LPM* acting as a cooling system is quite efficient and it indicates that the thermal model should be validated. Actually, if the rotor bar temperature is higher than in the thermal model the torque would be shifted as in figure 2.6 whereby other quantities would certainly be affected.
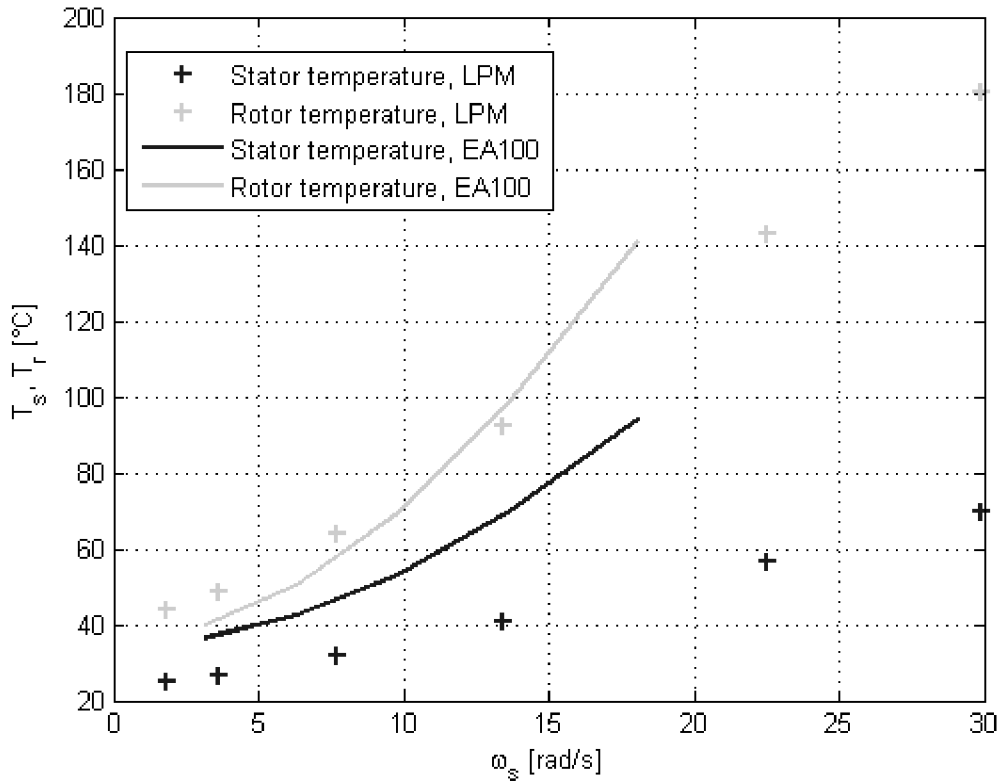
Figure 4.23: Comparison of stator and rotor conductor temperature over slip frequency (angular speed)

In this analysis, when the *LPM* with linear and non-linear material is compared, the difference is not so marginal; however it can be significant. Figure 4.24 shows the distribution of the magnetic flux. We should note that in this particular case the saturation occurs only in a few places. Nevertheless, rearranging the stator slots and rotor bars can lead to enlarging the saturated areas.
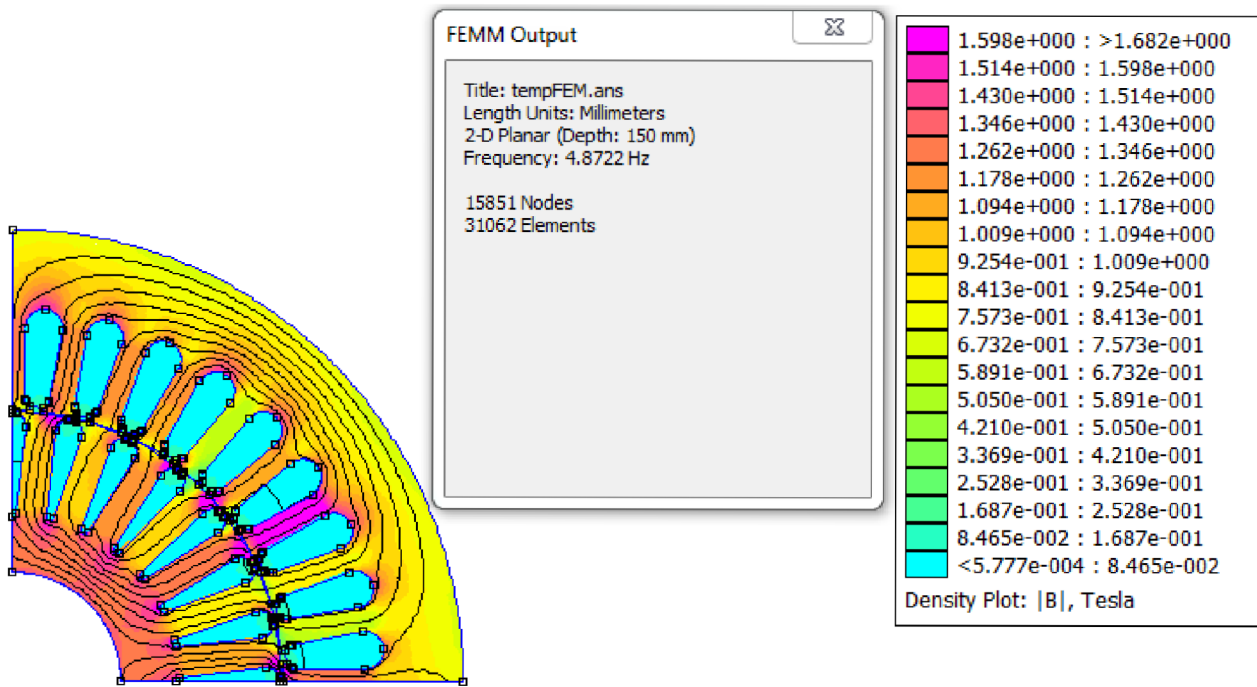
Figure 4.24: Flux distribution in the case of non-linear material

5 Evaluation of results

This section covers the results of the thesis as introduced and covered throughout the chapters above. In addition to this point, the chapter offers a few suggestions for future development.

5.1 Summary

In order to be able to analyze all the physical behavior inside the machine, literature research needed to be done is in chapter 2. Section 2.1 of this chapter describes the basics of induction machines including its construction, controlling, behavior and specific relations. The following section 2.2 covered the fundamental background of theory of electromagnetism required for the next section. The background also includes behavior of non-ideal materials and it also links to the *FEMM* analysis presented in section 2.3. The last section of this chapter dealt with thermal processes.

The aim of this thesis was the design of a complex model of an induction machine whereby an analysis of such a machine could be performed. The whole model consists of several sub-models such as electromagnetic, electric and thermal. The complex model is called *LPM* (lumped-parameter model) and its solution is in chapter 4. The basic structure of the proposed complex model is described in section 4.1.1. *LPM* offers saving of the model as well as editing it. *LPM* has its own independent group system which makes the working with blocks easier. The description of creating a new model and belonging files is in section 4.1.2. The *LPM* has a *New_GUI* (graphical user interface) which is used for assigning properties of *LPM* when creating a new model whereby the model settings become more comfortable for the user. Section 4.1.3 specifies additional parameters and conditions for the analysis that need to be set. For that reason, *LPM* has a *Solve_GUI* which is an interactive solver editor that facilitates the setting of additional parameters of the analysis. Section 4.1.4 deals with the connection to *FEMM* which is a program for solving electromagnetic problems.

The electromagnetic model is described in section 4.2. The model consists of, at first, an analysis of the machine using *FEMM* and also the further computation of machine parameters using *Matlab*. The model enables involving non-linear material in the analysis. *FEMM* solves only *2D* problems and thus there are lot of factors neglected. The flux leakage off the rotor end-rings cannot easily be modeled in a *2D* analysis. It also affects the relation between current and generated torque. Analogously, it is impossible to involve the flux leakage off the stator end-winding in a *2D* analysis. Usually, the rotor bars are skewed or multilayered which is also neglected here. The higher harmonic effects which can also cause losses are also impossible to analyze in *FEMM* analysis. Despite the fact that *FEMM* can compute the iron losses, the results obtained using the approach situated in appendix [4] were unfortunately significantly lower (hundredths) than the real values of these losses.

The electric model deals with computation of electric quantities in section 4.3. Section 4.3.1 describes an electric circuit in the case where non-linear material in the stator and rotor core is involved. Section 4.3.2 explains the configuration of three phase power supply and its effect on electric quantities. Section 4.3.3 deals with the estimation of resistances and inductances which occur in the electric circuit. The model includes an increase of rotor resistance due to rotor end-rings and analogously for stator resistance.

The thermal model, described in section 4.4, is a net of segments of the machine whereby the temperatures are obtained for the given heat losses matching to its segments. The model involves conduction heat transfer, convection and thermal contact heat transfer. Radiation has been neglected.

Section 4.5 deals with *LPM*. The process of *LPM* is described in section 4.5.1. The thermal model affects both the electric and the electromagnetic models via the stator and rotor resistances. Section 4.5.2 explains the calculation of quantities that interface the models. The stability of the *LPM* iterative process is covered in section 4.5.3. *LPM* has some useful features in terms of its capabilities. There is a library with user-defined materials in a *Matlab* file which is useful for adding, editing and, in the case of non-linear material, the setting of *B-H* relation. The model can be additionally edited using a *FEMM* window. Also, *LPM* enables simplifying the analyzed geometry into a partial area depending on the number of electromagnetic poles whereby the analysis becomes quicker.

LPM was successfully tested on the machine *TM2-100-4L* in section 4.6. The results are compared with results from analytical program *EA100* and with measured quantities of the machine at a steady-state after twelve hours of work and at a non-steady-state when the machine was cool. The results from *EA100* and *LPM* are close to one another. Nevertheless, they differ from the measured data. There are many factors that need to be taken into account, e.g. the neglect of flux leakage off rotor end-rings, neglect of flux leakage off stator end-winding, approximate estimation of electrical and thermal resistances, measurement conditions and method, age of machine, etc. Considering all these neglected factors, the results are quiet satisfying.

5.2 Suggestions for future development

This paper deals with several physical aspects of an induction machine that can be used as background for future developments. *LPM* combines three models and each of them can be extended. The electromagnetic model can be investigated in the case of a multilayered or skewed rotor cage. Also, it would be nice to calculate the real iron losses for non-linear material instead of estimating them. The electric model could be modeled via *Simscape Power System* in *Simulink* and supplemented with extra resistors representing the iron losses or multilayer rotor cage.

The *LPM* was dealing with a steady state of the machine; however, it would be interesting to explore a non-steady state at least regarding the thermal model. In that case, the thermal net would imply some thermal capacitances. Further exploration of this issue may aid in our ability to simulate the starting of the machine, overloading it or a malfunction of heating.

Bibliography

[1] Composition of induction machine. 2000. In: *Direct Industry* [online]. Marseille: VirtualExpo. [Accessed 5 May 2017]. Available at:
http://img.directindustry.com/images_di/photo-g/52755-3712277.jpg

[2] Výpočet asynchronního motoru. 1973. BRÁZDA, Miroslav and Rudolf STAŇA. *Výpočet asynchronního motoru.* Brno: Výzkumný a vývojový ústav elektrických strojů točivých, p. 222.

[3] KOPYLOV, Igor Petrovič. 1988. *Stavba elektrických strojů: celostátní vysokoškolská učebnice pro elektrotechnické fakulty vysokých škol technických.* Praha: Státní nakladatelství technické literatury.

[4] MEEKER, David. 2004. Induction motor example. In: *Femm* [online]. p. 13. [Accessed 3 May 2017]. Available at: http://www.femm.info/wiki/InductionMotorExample

[5] CLARKE, Richard. 2014. Producing wound components. In: *University of Surrey* [online]. Surrey, UK: University of Surrey. [Accessed 5 May 2017]. Available at:
http://info.ee.surrey.ac.uk/Workshop/advice/coils/index.html

[6] CIPÍN, Radoslav. 2012. *Moderní matematické metody syntézy a analýzy střídavých strojů.* Brno. Dissertation. BUT, Faculty of Electrical Engineering and Communication.

[7] MEEKER, David. 2015. *Finite element method magnetics version 4.2: User's Manual* [online]. [Accessed 6 May 2017]. Available at:
http://www.femm.info/Archives/doc/manual42.pdf

[8] CLARKE, Richard. 2008. Magnetic properties of materials. In: *University of Surrey* [online]. Surrey, UK: University of Surrey. [Accessed 5 May 2017]. Available at:
http://info.ee.surrey.ac.uk/Workshop/advice/coils/mu/index.html#mu

[9] CLARKE, Richard. 2008. Hysteresis loss. In: *University of Surrey* [online]. Surrey, UK: University of Surrey. [Accessed 5 May 2017]. Available at:
http://info.ee.surrey.ac.uk/Workshop/advice/coils/power_loss.html#hyst

[10] Nonlinear time harmonic hysteresis loss model. 2014. *Femm* [online]. [Accessed 7 May 2017]. Available at: http://www.femm.info/wiki/HysteresisLoss

[11] ÇENGEL, Yunus A. and Robert H. TURNER. c2005. *Fundamentals of thermal-fluid sciences.* 2nd ed. Boston: McGraw-Hill Companies. ISBN 00-724-5426-1.

[12] MEEKER, David. 2010. *Finite Element Method Magnetics: OctaveFEMM* [online]. [Accessed 15 May 2017]. Available at: http://www.femm.info/Archives/doc/octavefemm.pdf

List of figures

List of abbreviations and symbols

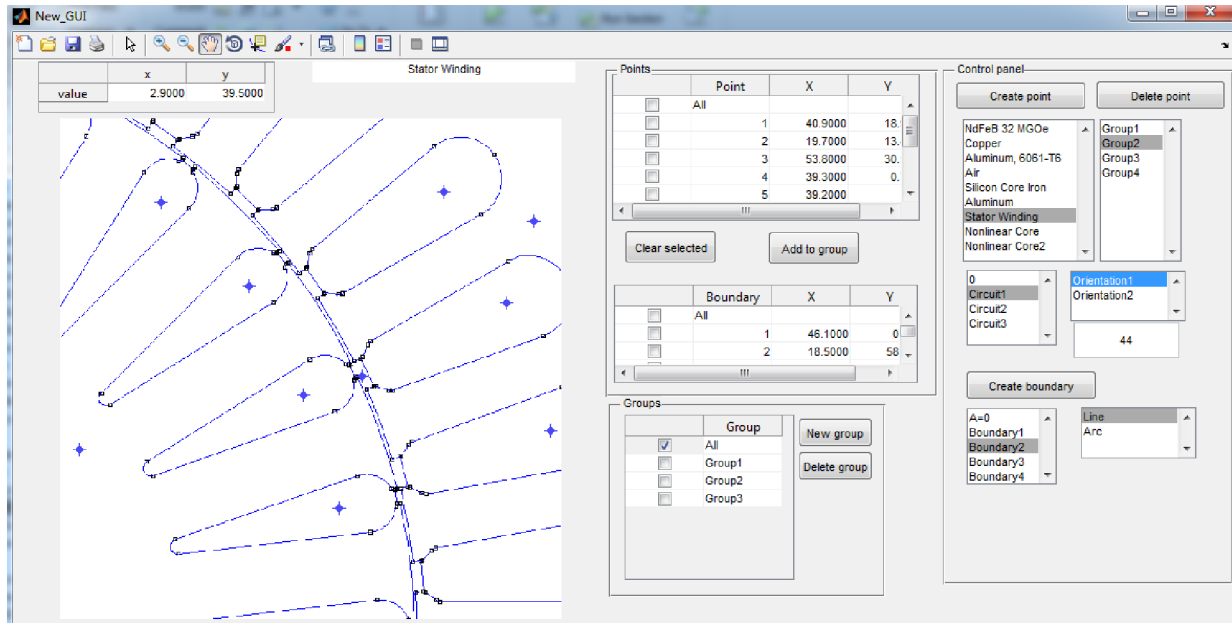|	
AC	Alternating Current
CAD	Computer Aided Design
FEA	Finite Element Analysis
FEM	Finite Element Method
FEMM	Finite Element Method Magnetics
GUI	Graphical User Interface
LPM	Lumped-Parameter Model
New_GUI	Editor used for creating a new model
RMS	Root Mean Square
Solve_GUI	Editor used for setting parameters of an analysis

Appendix

Figure A: Creating a new model

New_GUI is a graphical-user-interface for creating a new model. The figure above shows the imported geometry (figure 4.13) while the user can add the block properties to the enclosures, lines and arcs. The *GUI* also enables to zoom or pan within the geometry.
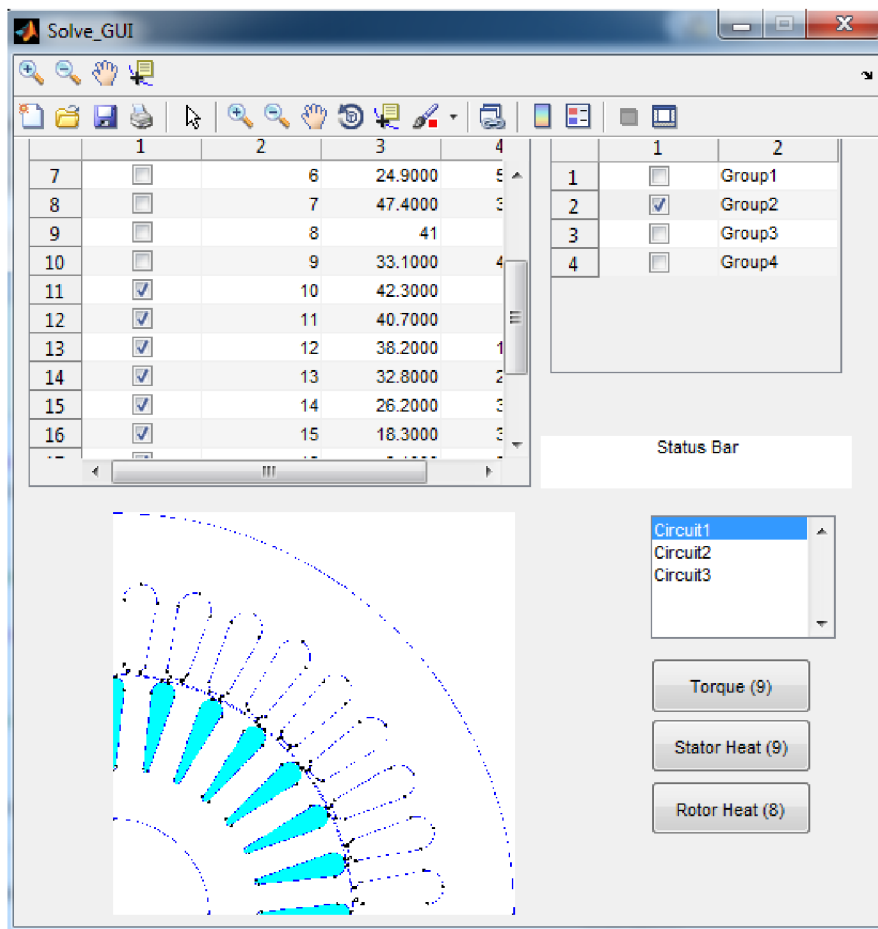
Figure B: Selection of block labels

A *Solve_GUI* file has been created in *Matlab* for setting analysis parameters. Using this *GUI* the user can define the range of slip frequencies, maximum count of iterations, stop-criterion of iterations, desired output power, and some selections of block labels for subsequent integrations which are furthered by *FEMM* postprocessor. The figure above shows the selection of block labels.